

# The universal rotation curve of low surface brightness galaxies – IV. The interrelation between dark and luminous matter

Chiara Di Paolo,<sup>1,2,3★</sup> Paolo Salucci<sup>1,2,3★</sup> and Adnan Erkurt<sup>4</sup>

<sup>1</sup>*Physics, SISSA/ISAS, Via Bonomea 265, I-34136 Trieste, Italy*

<sup>2</sup>*INFN Sez. Trieste, Via A. Valerio 2, I-34127 Trieste, Italy*

<sup>3</sup>*IFPU, Via Beirut 2-4, I-34151 Trieste, Italy*

<sup>4</sup>*Physics, Istanbul University, Beyazit, 34452 Fatih/Istanbul, Turkey*

Accepted 2019 September 17. Received 2019 August 2; in original form 2018 October 4

## ABSTRACT

We investigate the properties of the baryonic and the dark matter components in low surface brightness (LSB) disc galaxies, with central surface brightness in the  $B$  band  $\mu_0 \geq 23$  mag arcsec<sup>-2</sup>. The sample is composed of 72 objects, whose rotation curves show an orderly trend reflecting the idea of a universal rotation curve (URC) similar to that found in the local high surface brightness (HSB) spirals in previous works. This curve relies on the mass modelling of the co-added rotation curves, involving the contribution from an exponential stellar disc and a Burkert cored dark matter halo. We find that the dark matter is dominant especially within the smallest and less luminous LSB galaxies. Dark matter haloes have a central surface density  $\Sigma_0 \sim 100 M_\odot \text{pc}^{-2}$ , similar to galaxies of different Hubble types and luminosities. We find various scaling relations among the LSBs structural properties which turn out to be similar but not identical to what has been found in HSB spirals. In addition, the investigation of these objects calls for the introduction of a new luminous parameter, the stellar compactness  $C_*$  (analogously to a recent work by Karukes & Salucci), alongside the optical radius and the optical velocity in order to reproduce the URC. Furthermore, a mysterious entanglement between the properties of the luminous and the dark matter emerges.

**Key words:** galaxies: fundamental parameters – galaxies: kinematics and dynamics – dark matter.

## 1 INTRODUCTION

Dark matter (DM) is the main actor in cosmology. It is believed to constitute the great majority of the mass and to rule the processes of structure formation in the Universe.<sup>1</sup> The so-called Lambda cold dark matter ( $\Lambda$ CDM) scenario, in which one assumes a weakly interacting massive particle (WIMP) that decouples from the primordial plasma when non-relativistic, successfully reproduces the structure of the cosmos on large scales (Kolb & Turner 1990). However, some challenges to this scenario emerge at small galactic scales, such as the ‘missing satellite problem’ (e.g. Klypin et al. 1999; Moore et al. 1999; Zavala et al. 2009; Papastergis et al. 2011; Klypin et al. 2015) and the ‘too-big-to-fail problem’ (e.g. Boylan-Kolchin, Bullock & Kaplinghat 2012; Ferrero, Navarro & Sales 2012; Garrison-Kimmel et al. 2014; Papastergis et al. 2015). Moreover, the galactic inner DM density profiles generally appear to be cored, rather than cuspy as predicted in the  $\Lambda$ CDM scenario (e.g.

Salucci 2001; de Blok & Bosma 2002; Gentile et al. 2004, 2005; Simon et al. 2005; Del Popolo & Kroupa 2009; Oh et al. 2011; Weinberg et al. 2015), in spirals of any luminosity (see Salucci 2019). In ellipticals and dwarf spheroidals (dSphs) the question is still uncertain (Salucci 2019).

These issues suggest to study different scenarios from the ‘simple’  $\Lambda$ CDM, such as warm DM (e.g. de Vega et al. 2013; Lovell et al. 2014), self-interacting DM (e.g. Vogelsberger et al. 2014; Elbert et al. 2015), or to introduce the effect of the baryonic matter feedbacks on the DM distribution (e.g. Navarro, Eke & Frenk 1996; Read & Gilmore 2005; Mashchenko, Couchman & Wadsley 2006; Di Cintio et al. 2014; Pontzen & Governato 2014).

One important way to investigate the properties of DM in galaxies is to study rotation-supported systems, such as spiral galaxies, since they have a rather simple kinematics. The stars are mainly distributed in an exponential thin disc with scale length  $R_d$  (Freeman 1970). Notice that related to this scale length, in this paper, we will use the optical radius  $R_{\text{opt}}$ , defined as the radius encompassing 83 per cent of the total luminosity and proportional to the stellar disc scale length:  $R_{\text{opt}} = 3.2R_d$  (the details of this choice are expressed at length in Persic, Salucci & Stel 1996). In order to explain the

\* E-mail: [cdipaolo@sisa.it](mailto:cdipaolo@sisa.it) (CDP); [salucci@sisa.it](mailto:salucci@sisa.it) (PS)

<sup>1</sup>In this paper we adopt the scenario of DM in Newtonian gravity, leaving to other works the investigation in different frameworks.

observed rotation curves (RCs) of disc systems, it is necessary to assume the presence of a spherical DM halo surrounding the galaxies (Faber & Gallagher 1979; Rubin et al. 1985; Salucci 2019).

A very interesting feature of spiral galaxies is that the bigger they are, the more luminous they are and the higher rotational velocities they show. Moreover, when their RCs, with the radial coordinate normalized with respect to their optical radius  $R_{\text{opt}}$ , are put together, they appear to follow a *universal trend* (first shown in fig. 4 in Rubin et al. 1985, then in Persic & Salucci 1991, Persic et al. 1996, Rhee 1996, Roscoe 1999, Catinella, Giovanelli & Haynes 2006, Noordermeer et al. 2007, Salucci et al. 2007, López Fune 2018, and Salucci 2019). From small to large galaxies, the RCs have higher and higher velocities and profiles that gradually change. See also the top panel in Fig. A1 in Appendix A.

By means of the ‘*universal rotation curve* (URC) method’, which involves groupings of similar RCs and their mass modelling, it is possible to construct an analytic function that gives a good description of all the RCs of the local spiral galaxies within a spherical volume  $\simeq (100 \text{ Mpc})^3$ . The URC method was applied for the first time in Persic & Salucci (1991). This was followed by a series of three works: Persic et al. (1996) (Paper I), Salucci et al. (2007) (Paper II), and Karukes & Salucci (2017) (Paper III), where the URC method gave deeper results related to *normal spirals*, also called high surface brightness (HSB) spirals, and *dwarf disc* (*dd*) galaxies. A subsequent work confirmed the above results with up to 3100 disc galaxies and highlighted the existence of *tight scaling relations* among the properties of spirals with different size (Lapi, Salucci & Danese 2018).

Let us underline that the concept of *universality* in the RCs means that all of them can be described by the same analytical function as long as expressed in terms of the normalized radius and of one global parameter of the galaxies, such as magnitude, luminosity, mass, or velocity at the optical radius ( $V_{\text{opt}} \equiv V(R_{\text{opt}})$ ). Therefore, the URC is the circular velocity at a certain radius  $r$  given by  $V(r/R_{\text{opt}}, L)$ , where  $L$  is the galaxy’s luminosity. See the bottom panel in Fig. A1 in Appendix A. Obviously, the URC does not change even using, instead of  $R_{\text{opt}}$ , any other radial coordinate proportional to the stellar disc scale length  $R_d$ .<sup>2</sup>

The URC is a very powerful tool since, given the observation of few properties (such as  $R_d$  and  $L$ ) of a certain galaxy, it is possible to deduce its RC and all its properties.

In this paper (IV), we investigate the concept of the URC, the resulting mass models, and the scaling relations in *low surface brightness* (LSB) disc galaxies, comparing them to the results of other disc galaxies of a different Hubble type.

LSB galaxies are rotating disc systems which emit an amount of light per area smaller than normal spirals. They are locally more isolated than other kinds of galaxies (e.g. Bothun et al. 1993; Rosenbaum & Bomans 2004) and likely evolving very slowly with very low star formation rates. This is suggested by colours, metallicities, gas fractions, and extensive population synthesis modelling (e.g. van der Hulst et al. 1993; McGaugh 1994; de Blok, van der Hulst & Bothun 1995; Bell et al. 2000). As we see in radio synthesis observations, LSB galaxies have extended gas discs with low gas surface densities and high  $M_{\text{HI}}/L$  ratios (e.g. van der Hulst et al. 1993), where  $M_{\text{HI}}$  is the mass of the H I gaseous disc. The low metallicities make the gas cooling difficult and in turn the stars difficult to form (e.g. McGaugh 1994). LSBs are required to

be dominated by DM, as shown by the analysis of their Tully–Fisher relation (e.g. Zwaan et al. 1995) and of their individual RCs (e.g. de Blok, McGaugh & Rubin 2001; de Blok & Bosma 2002).

The LSB sample used in this work involves 72 galaxies selected from literature, whose optical velocities span from  $\sim 24$  to  $\sim 300 \text{ km s}^{-1}$ , covering the values of the full population. Our analysis of LSBs by means of the URC method is triggered by the result shown in Fig. 1, from which we can see that the LSBs RCs gradually change very orderly from small to large galaxies (or equally from objects with small to large optical velocities  $V_{\text{opt}}$ ). Following the URC method, the sample of galaxies is divided in different velocity bins, according to their increasing values of  $V_{\text{opt}}$ . A double normalization of all the RCs is performed with respect to: (i) their own  $R_{\text{opt}}$ , along the radial axis, and (ii) their own  $V_{\text{opt}}$ , along the velocity axis. In these specific coordinates, in each velocity bin, the RCs are all alike. Then, the double-normalized co-added RCs, a kind of average RC for each velocity bin, are constructed. The analysis continues with their *mass modelling*, yielding the distribution of luminous and DM in structures with different  $V_{\text{opt}}$ . This is followed by the denormalization process, which gives the structural parameters of each object of the sample, and allows us to obtain the related scaling relations for the LSBs. The internal scatter of the found scaling relationships is larger (three times or more) than the analogous ones in normal spirals. A similar finding also emerged in the case of *dd* galaxies (Karukes & Salucci 2017). Remarkably, the scatter in the *dd* relationships was reduced after the introduction of a new quantity, the *compactness* of the luminous matter distribution  $C_*$ , that indicates how the values of  $R_d$  vary in galaxies with the same stellar disc mass. Therefore, such results statistically suggest the introduction of the compactness also in the analogous LSBs scaling relationships. The previous steps lead to the construction of the URC for the LSBs, which is one of the main goals of this work. Finally, in analogy to Karukes & Salucci (2017), we also investigate the compactness of the DM distribution  $C_{\text{DM}}$  and its relation to  $C_*$ .

The structure of this paper is as follows: in Section 2, we describe our sample of LSB galaxies; in Sections 3–5, the URC method and the analysis of the LSBs structural properties are described in detail; in Section 6 we obtain the LSBs scaling relations and we compare them to those of other disc systems; in Sections 7–8, the concept of *compactness* is introduced and the URC-LSB is built; finally, in Section 9, we comment on our main results.

The distances are evaluated from the recessional velocity assuming  $H_0 = 72 \text{ km s}^{-1} \text{ Mpc}^{-1}$ .

## 2 THE LSB SAMPLE AND THE ROTATION CURVES UNIVERSAL TREND

We consider 72 rotating disc galaxies classified as ‘low surface brightness’ in literature (see Table B1 in Appendix B). In the very majority of cases the authors classify a galaxy as LSB when the face-on central surface brightness  $\mu_0 \gtrsim 23 \text{ mag arcsec}^{-2}$  in the B band. We select our sample according to the following criteria:

- (i) the RCs extend to at least  $\simeq 0.8 R_{\text{opt}}$  (when  $V_{\text{opt}}$  is not available from observation, it can be extrapolated since from  $\simeq 1/2 R_{\text{opt}}$  to  $2 R_{\text{opt}}$ , the RCs are linear in radius with a small value of the slope);
- (ii) the RCs are symmetric, smooth (e.g. without strong signs of non-circular motions) and with an average fractional internal uncertainty lesser than 20 per cent. In short we eliminated RCs that in no way can be mass-modelled without huge uncertainties;

<sup>2</sup>The results of the paper remain unchanged for any chosen radial coordinate if expressed in units of  $\lambda R_d$ , with any  $\lambda$  value ranging from one to four.

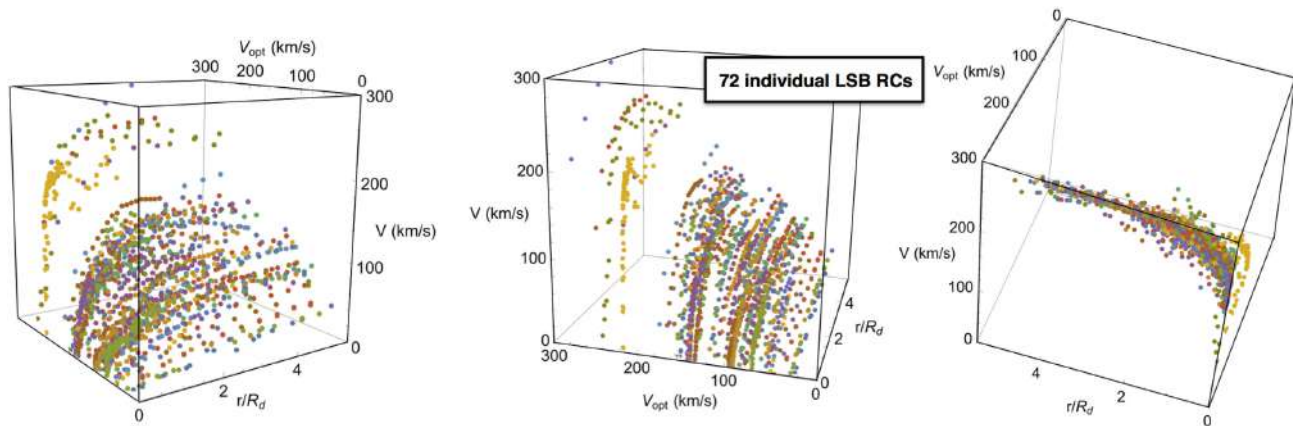


**Figure 1.** LSBs RCs (each one in different colour) ordered according to increasing optical velocities  $V_{\text{opt}}$ . Note that the radial coordinate is normalized with respect to the disc scale length  $R_d$ . A *universal trend* is recognizable analogous to that emerged in normal spirals (see Fig. A1 in Appendix A).

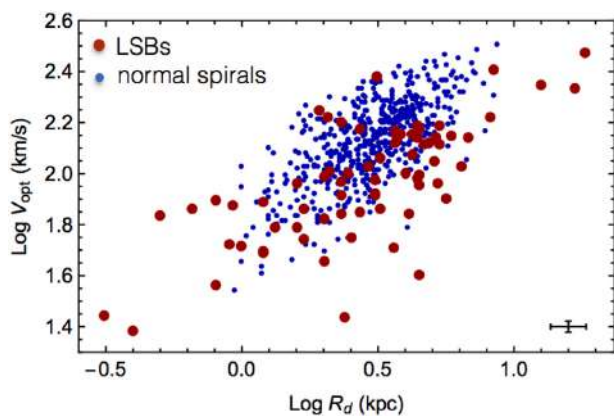


**Figure 2.** Optical velocity versus disc scale lengths in LSB galaxies (*red*) and in normal spirals (*blue*) (Persic et al. 1996). The typical fractional uncertainties are 5 per cent in  $V_{\text{opt}}$  and 15 per cent in  $R_d$ , as shown in the bottom right corner.

(iii) the galaxy disc scale length  $R_d$  and the inclination function  $1/\sin i$  are known within 30 per cent uncertainty.

The selected 72 LSBs have optical velocities  $V_{\text{opt}}$  spanning from  $\sim 24$  to  $\sim 300 \text{ km s}^{-1}$ ; the sample of RCs consists of 1614 independent  $(r, V)$  measurements. When the RCs, expressed in normalized radial units, are put together, see Fig. 1, they show a universal trend analogous to that of the normal spirals (Fig. A1 in Appendix A). Then, given the observed trend in LSBs and the relevance of the URC method, we search our sample of LSBs for a URC and for the related scaling relations among the galaxy’s structural parameters.

In Fig. 2, the values of the stellar disc scale lengths  $R_d$  and the optical velocities  $V_{\text{opt}}$  measured in LSBs are shown and compared to those measured in normal spirals. A larger spread in the former case is clearly recognizable. This feature will be used later to explain the need of introducing a new structural variable: the *compactness*.

Finally, it is useful to stress that previous studies on individual LSB galaxies reveal in the mass profiles of these objects the presence of an exponential stellar disc, an extended gaseous disc at very low density (e.g. de Blok, McGaugh & van der Hulst 1996), and the presence of a spherical DM halo, likely with a core profile (e.g. de Blok et al. 2001; de Blok & Bosma 2002; Kuzio de Naray, S. & de Blok 2008).

### 3 THE CO-ADDED ROTATION CURVES OF LSB GALAXIES

The individual RCs (in normalized radial units) shown in Fig. 1 motivate us to proceed, also in LSB, with the URC method, analogously to what has been done on the HSB spiral galaxies (Persic et al. 1996; Lapi et al. 2018) and dwarf discs (Karukes & Salucci 2017). It is useful to anticipate here that the average scatter of the RCs data from a fitting surface (as the URC in Fig. 15) is  $\Delta V / V \simeq 8$  per cent (taking into account the observational errors, the systematics, and the small non-circularities in the motion). This small value gives an idea of the universality of the LSBs RCs expressed in normalized radial units.

Among the first steps, the URC method (Persic et al. 1996) requires to make the galaxies RCs as similar as possible (in radial extension, amplitude, and profile) by introducing the normalization of their coordinates and an eventual galaxies binning. Let us notice that the justification for these starting steps comes from the analogous process performed in spirals and from a qualitative inspection of LSB RCs. Finally, the goodness of the results will show the goodness of the method.

The characteristics of the RCs in physical and normalized units are visible in Fig. 3:

- (i) in the first panel, the RCs are expressed in physical units; they appear to be different in radial extension, amplitude, and profile;
- (ii) in the second panel, the RCs are expressed in normalized radial units with respect to their disc scale length  $R_d$ . Their radial extensions are made more similar. Indeed, most of the data are extended up to  $\simeq 5.5R_d$ ;
- (iii) in the third panel, the RCs are expressed in double-normalized units with respect to their disc scale length  $R_d$  and optical velocity  $V_{\text{opt}}$ , along the radial and the velocity axis, respectively. The RCs in such specific units are comparable also in their amplitude.

Overall, the double normalization makes the 72 RCs more similar, apart from their profiles. However, when these RCs are arranged in five optical velocity bins according to their increasing  $V_{\text{opt}}$  as in Fig. 4, we realize that the *double-normalized* RCs profiles belonging to one of these bins are very similar among themselves but clearly different from those of the RCs in other optical velocity bins (see Fig. 5).

We have chosen to build five  $V_{\text{opt}}$  bins as a compromise between having a large number of data for each co-added RC and a large

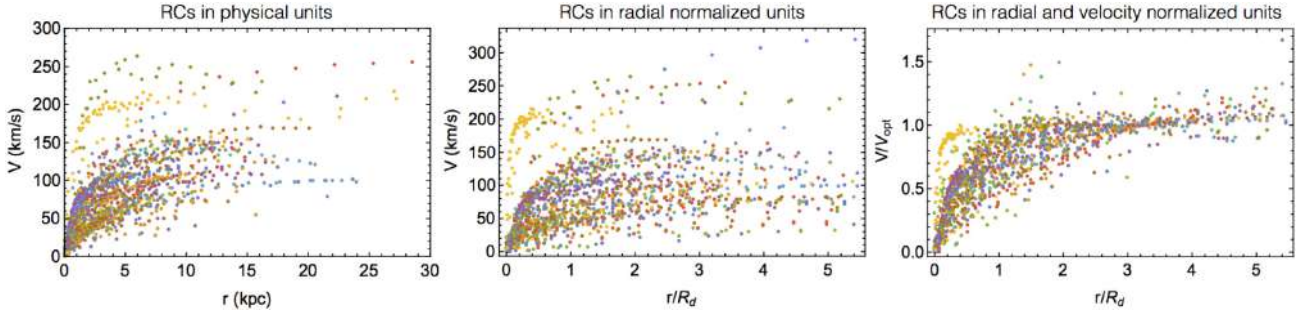


**Figure 3.** LSBs RCs (each one in different colour) in physical units (*first panel*), in normalized radial units (*second panel*), and in double-normalized radial and velocity units (*third panel*). See also Appendix C.

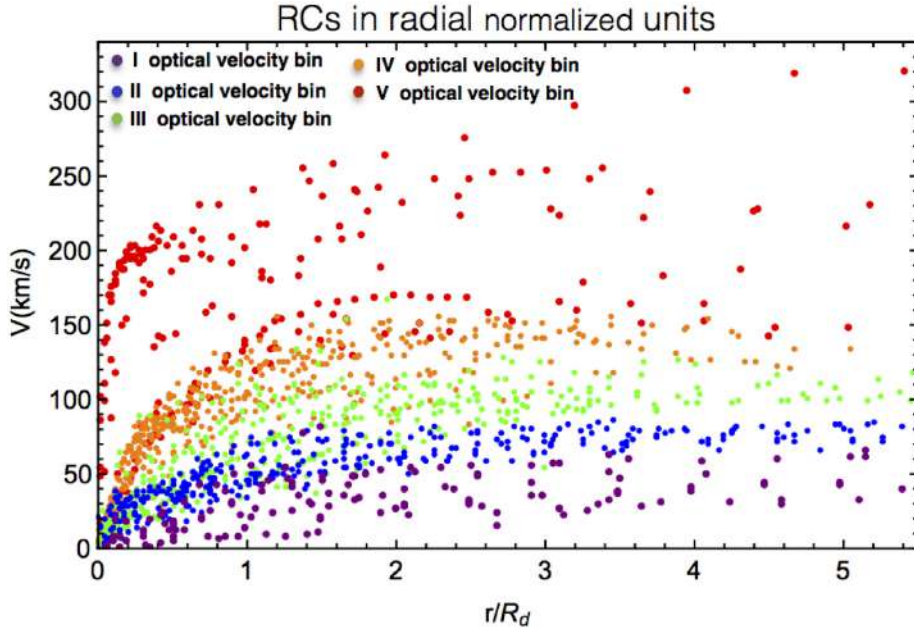


**Figure 4.** LSBs RCs (in normalized radial units) grouped in five optical velocity bins. In this and in the following figures, *purple, blue, green, orange, and red* colours are referred to the RCs of the I, II, III, IV, and V optical velocity bins, respectively.

number of co-added RCs. Particularly, the binning in five groups is suggested by the fact that, since the sample includes 72 objects, 10–15 galaxies are the minimum number in each optical velocity bin in order to create suitable co-added RCs (that will be described in the next paragraphs) and to eliminate statistically observational errors and small non-circularities from the individual RCs.

In detail, the number of galaxies in each bin, the span in  $V_{\text{opt}}$ , the average optical velocity  $\langle V_{\text{opt}} \rangle$ , the average stellar disc scale length  $\langle R_d \rangle$ , the number of galaxies and of the  $(r, V)$  data are all reported in Table 1.

We also point out Fig. D1 in Appendix D, where the RCs, grouped in their velocity bins, are compared in physical and double-normalized units.

After that all the RCs are double normalized, we perform the *radial binning* in each of the five *optical velocity bins*. Similar to the velocity binning process, we have chosen  $\approx 11$  normalized radial bins as a compromise between having a large number of data for each radial bin and a large number of radial bins for each co-added RC. Moreover, we required that the inner radial bins (for  $r \leq 2R_d$ ) and the outer radial bins (for  $r > 2R_d$ ) included a minimum of 13 and five measurements, respectively. In detail, for the I, the II, and the III optical velocity bins, the radial *normalized* coordinate is divided in

12 bins: the first five have a width of 0.4 and the remaining a width of 0.5. For the IV and the V velocity bins, for statistical reasons, we adopt a different division of the radial coordinate. In the IV velocity bin we adopt three radial bins of width 0.4, five of width 0.6, and the last one of width 1. In the V velocity bin, we adopt five, four, and two radial bins of widths 0.4, 0.5, and 0.8, respectively. The number of data per radial bin is reported in Tables E1–E2 in Appendix E. Reasonable variations of the positions and amplitudes of the radial bins do not affect the resulting co-added RCs.

Therefore, for each of the five  $V_{\text{opt}}$  bins, in every  $k$ -radial bin we built there are  $N_k$  double-normalized velocities  $v_{ik}$ , with  $i$  running from 1 to  $N_k$ . Their average value is given by  $V_k = \frac{\sum_{i=1}^{N_k} v_{ik}}{N_k}$ , as in Persic et al. (1996). Then, by repeating this for all the radial bins of each of the five  $V_{\text{opt}}$  bins, we obtain the five double-normalized *co-added* RCs shown in Fig. 5. The *standard error of the mean* we consider in this work is

$$\delta V_k = \sqrt{\frac{\sum_{i=1}^{N_k} (v_{ik} - V_k)^2}{N_k(N_k - 1)}}. \quad (1)$$

In short, the above co-added RCs can be considered as the average RCs of galaxies of similar properties as e.g.  $V_{\text{opt}}$ . It is

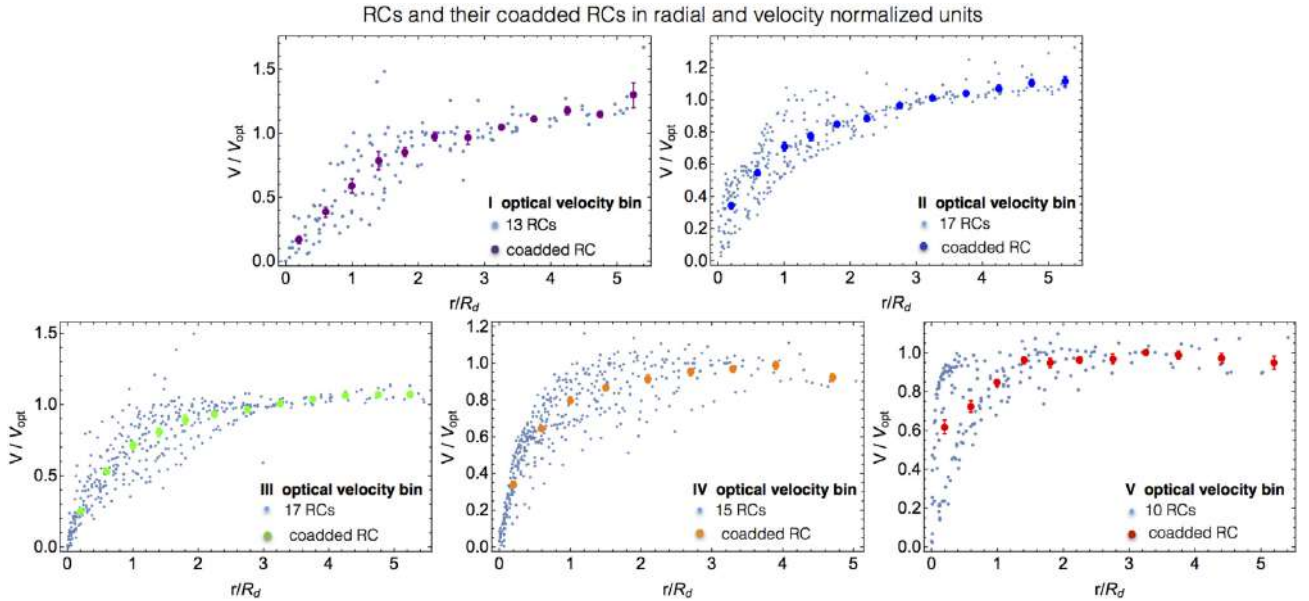


**Figure 5.** In each of the five panels: LSBs double-normalized RCs for each of the five optical velocity bins (*grey points*). Also shown are the corresponding co-added RCs (*larger coloured points*) for each of these five bins. Notice that part of the scatter in the five profiles will be eliminated by introducing the compactness in the URC. See Section 7.

**Table 1.** LSB velocity bins. Columns: (1)  $i$  - velocity bin; (2) range values for  $V_{\text{opt}}$ ; (3) number of LSB galaxies in each velocity bin; (4) average value of  $V_{\text{opt}}$  evaluated from the individual galaxies; (5) average value of  $R_d$  evaluated from the individual galaxies; (6) number of  $(r, V)$  data from the individual galaxies.

$V_{\text{opt}}$ bin	$V_{\text{opt}}$ range $\text{km s}^{-1}$	N. galaxies	$\langle V_{\text{opt}} \rangle$ $\text{km s}^{-1}$	$\langle R_d \rangle$ kpc	N. data
(1)	(2)	(3)	(4)	(5)	(6)
1	24–60	13	43.5	1.7	151
2	60–85	17	73.3	2.2	393
3	85–120	17	100.6	3.7	419
4	120–154	15	140.6	4.5	441
5	154–300	10	205.6	7.9	210

worth emphasizing the advantages of these RCs: their building erases the peculiarities and also reduces the observational errors of the individual RCs. This yields to a universal description of the kinematics of LSBs by means of five extended and smooth RCs whose values have an uncertainty at the level of 5–15 per cent. In Fig. 6 the five co-added RCs are shown together.

(i) in the first panel, they are expressed in double-normalized units covering a very small region in the  $(V/V_{\text{opt}}, R/R_{\text{opt}})$  plane;

(ii) in the second panel, they are expressed in physical velocity units. These co-added RCs are obtained by multiplying the previous co-added RCs by the corresponding  $\langle V_{\text{opt}} \rangle$  (reported in Table 1).

(iii) in the third panel, the co-added RCs are expressed in physical units both along the velocity and the radial axes. They are obtained by multiplying the previous co-added RCs by the corresponding  $\langle R_d \rangle$  reported in Table 1.

In Fig. 6 the difference in the profiles corresponding to galaxies with different optical velocities is evident.<sup>3</sup>

<sup>3</sup>This is explained by the very different luminous and dark mass distributions in LSBs of different sizes and optical velocities, as shown in the next section.

All the data shown in Fig. 6 can be recast by means of Tables E1–E2 (in Appendix E) and Table 1.

#### 4 THE MASS MODELLING OF THE CO-ADDED ROTATION CURVES

In this section we investigate the co-added RCs, normalized along the radial axis (see second panel in Fig. 6), whose data are listed in Tables E1–E2 in Appendix E. We model the co-added RCs data, as in normal spirals (Salucci et al. 2007), with an analytic function  $V(r)$  which includes the contributions from the stellar disc  $V_d$  and from the DM halo  $V_h$ :

$$V^2(r) = V_d^2(r) + V_h^2(r). \quad (2)$$

Let us stress that in first approximation the inclusion in the model of a HI gaseous disc component can be neglected. In fact, the gas contribution is usually a minor component to the circular velocities, since the inner regions of galaxies are dominated by the stellar component and in the external regions, where the gas component overcomes the stellar one, the DM contribution is largely the most important (Evoli et al. 2011). A direct test in Appendix F shows that our assumption does not affect the mass modelling obtained in this paper.

We describe the stellar and the DM component. The first one is given by the well-known Freeman disc (Freeman 1970), whose surface density profile is

$$\Sigma_d(r) = \frac{M_d}{2\pi R_d^2} \exp(-r/R_d), \quad (3)$$

where  $M_d$  is the disc mass. Equation (3) leads to (Freeman 1970):

$$V_d^2(r) = \frac{1}{2} \frac{G M_d}{R_d} \left( \frac{r}{R_d} \right)^2 (I_0 K_0 - I_1 K_1), \quad (4)$$

where  $I_n$  and  $K_n$  are the modified Bessel functions computed at  $1.6x$ , with  $x = r/R_{\text{opt}}$ .

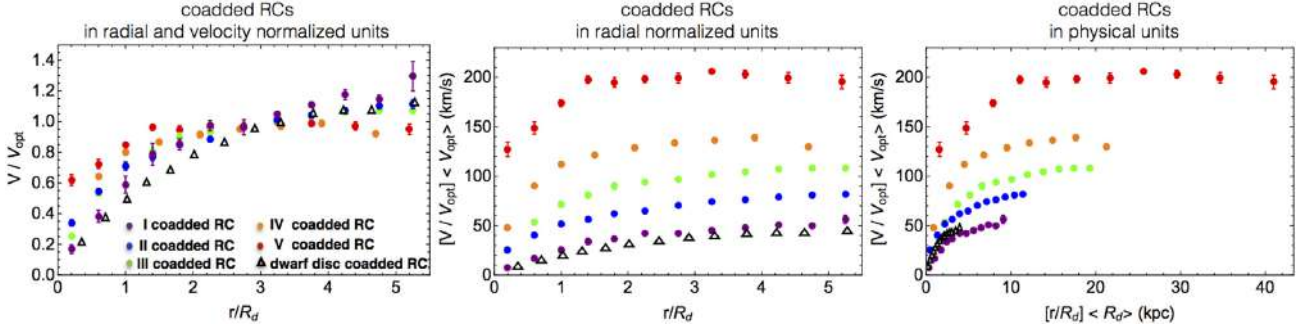


**Figure 6.** Co-added RCs for the five velocity bins in double-normalized units (*first panel*), in physical velocity units (*second panel*), and in physical units along both the velocity and radial axes (*third panel*). The black empty triangles are the co-added RC for the dwarf disc galaxies (Karukes & Salucci 2017).

Finally, for the fifth optical velocity bin we will introduce a bulge component (Das 2013).

Concerning the DM component, the presence of cored profiles in LSBs is well known from individual RCs (see e.g. de Blok et al. 2001; de Blok & Bosma 2002; Kuzio de Naray et al. 2008, Bullock & Boylan-Kolchin 2017). In this paper, we model the DM halo profile by means of the *cored Burkert profile* (Burkert 1995; Salucci & Burkert 2000). This halo profile has an excellent record in fitting the actual DM haloes around disc systems of any luminosity and Hubble Types (see Memola, Salucci & Babic 2011; Salucci et al. 2012; Lapi et al. 2018; Salucci 2019). In addition, the Burkert profile is in agreement with weak lensing data at virial distances (Donato et al. 2009).

It is however worth noticing that there is no sensible difference, in the mass modelling inside  $R_{\text{opt}}$ , in adopting different cored DM density profiles (Gentile et al. 2004). Then, we adopt the following density profile (Burkert 1995):

$$\rho_{\text{DM}}(r) = \frac{\rho_0 R_c^3}{(r + R_c)(r^2 + R_c^2)}, \quad (5)$$

where  $\rho_0$  is the central mass density and  $R_c$  is the core radius. Its mass distribution is

$$\begin{aligned} M_{\text{DM}}(r) &= \int_0^r 4\pi \tilde{r}^2 \rho_{\text{DM}}(\tilde{r}) d\tilde{r} = \\ &= 2\pi \rho_0 R_c^3 [\ln(1 + r/R_c) \\ &\quad - r/R_c + 0.5 \ln(1 + (r/R_c)^2)]. \end{aligned} \quad (6)$$

The contribution to the total circular velocity is given by

$$V_h^2(r) = G \frac{M_{\text{DM}}(r)}{r}. \quad (7)$$

We fit the five co-added RCs by means of the URC model described above, which, for each co-added RC, is characterized by three free parameters,  $M_d$ ,  $\rho_0$ , and  $R_c$ , all set to be larger than zero. Other limits for the priors of the fitting arise from the amplitude and the profile of the co-added RCs themselves. We require that:  $10^6 M_\odot \lesssim M_d \lesssim 10^{12} M_\odot$  from the galaxies luminosities,  $R_c \lesssim 200 \frac{R_{\text{opt}}}{30 \text{ kpc}}$  kpc to avoid solid body RCs in all objects, and  $10^{-26} \lesssim \rho_0 \lesssim 10^{-22} \text{ g cm}^{-3}$  (the lower limit guarantees that the dark component is able to fit the RC allied with the luminous component, the upper limit is to make the DM contribution important but not larger than the RCs amplitudes). Notice that these limits agree well with the outcomes of the modelling of individual RCs as found in literature.

The resulting best-fitting values for the three free parameters ( $M_d$ ,  $\rho_0$ ,  $R_c$ ) are reported in Table 2 and the best-fitting velocity models

are plotted alongside the co-added RCs in Fig. 7.

In the case of the V velocity bin, we introduce a central bulge (whose presence is typical in the largest galaxies) (Das 2013). We adopt for the bulge velocity component the simple functional form:

$$V_b^2(r) = \alpha_b V_{\text{in}}^2 \left( \frac{r}{r_{\text{in}}} \right)^{-1}, \quad (8)$$

where  $V_{\text{in}} = 127 \text{ km s}^{-1}$  and  $r_{\text{in}} = 0.2 \langle R_d \rangle \simeq 1.6 \text{ kpc}$  are the values of the first velocity point of the V co-added RC. Since  $r_{\text{in}}$  is larger than the edge of the bulge, we consider the latter as a point mass.  $\alpha_b$  is a parameter which can vary from 0.2 to 1 (e.g. see Yegorova & Salucci 2007). By fitting the V co-added RC we found:  $\alpha_b = 0.8$ ; the other best-fitting parameters  $M_d$ ,  $\rho_0$ ,  $R_c$  are reported in Table 2.

In Fig. 7 we realize that, in the inner regions of the LSB galaxies, the stellar component (dashed line) is dominant, while, on the contrary, in the external regions, the DM component (dot-dashed) is the dominant one. Moreover, the transition radius<sup>4</sup> between the region dominated by the baryonic matter and the region dominated by the DM increases with normalized radius when we move from galaxies with the lowest  $V_{\text{opt}}$  to galaxies with the highest  $V_{\text{opt}}$ . A similar behaviour was also observed in normal spiral galaxies (Persic et al. 1996; Lapi et al. 2018).

## 5 DENORMALIZATION OF THE CO-ADDED ROTATION CURVES

The mass models found in the previous section provided us with the structural parameters of the five co-added RCs. Now, we retrieve the properties from the individual RCs by means of the *denormalization* method. It relies on the facts that, in each velocity bin, (i) all the double-normalized RCs are similar to their co-added double-normalized RC (see Fig. 5) and that (ii) we have performed extremely good fits of the co-added RCs (see Fig. 7). Thus, the relations existing for the co-added RCs are assumed to approximately hold also for the individual RCs that form each of the five co-added ones.

The first relation that we apply in the denormalization process is shown in Fig. 8; the stellar disc scale length and the DM core radius of the five velocity models are strongly correlated. The best linear fit in logarithmic scale is

$$\text{Log } R_c = 0.60 + 1.42 \text{ Log } R_d. \quad (9)$$

<sup>4</sup>The *transition radius* is the radius where the DM component, dot-dashed line, overcomes the luminous component, dashed line.

**Table 2.** Relevant parameters of the five co-added RCs. Columns: (1)  $i$  - velocity bin; (2) average value of  $V_{\text{opt}}$ ; best-fitting value of (3)  $\rho_0$ ; (4)  $R_c$ ; (5)  $M_d$ ; (6) estimated halo virial mass according to equation (13); (7) fraction of baryonic component at  $R_{\text{opt}}$  (equation 11); (8)  $k$  values defined according to equation (10).

Vel. bin	$\langle V_{\text{opt}} \rangle$ km s $^{-1}$	$\rho_0$ 10 $^{-3}$ M $_{\odot}$ pc $^{-3}$	$R_c$ kpc	$M_d$ 10 $^{11}$ M $_{\odot}$	$M_{\text{vir}}$ 10 $^{11}$ M $_{\odot}$	$\alpha(R_{\text{opt}})$	$k$
(1)	(2)	(3)	(4)	(5)	(6)	(7)	(8)
1	43.5	3.7 $\pm$ 1.4	10.7 $\pm$ 4.3	(8.8 $\pm$ 1.8) $\times$ 10 $^{-3}$	1.0 $\pm$ 0.4	0.37	0.36
2	73.3	5.1 $\pm$ 1.1	12.8 $\pm$ 3.0	(3.8 $\pm$ 0.3) $\times$ 10 $^{-2}$	2.4 $\pm$ 0.9	0.49	0.44
3	100.6	3.7 $\pm$ 0.5	17.1 $\pm$ 1.9	(13.0 $\pm$ 0.5) $\times$ 10 $^{-2}$	4.0 $\pm$ 1.3	0.52	0.47
4	140.6	1.7 $^{+1.8}_{-1.1}$	30 $^{+40}_{-22}$	(4.2 $\pm$ 0.4) $\times$ 10 $^{-1}$	8.4 $\pm$ 3.5	0.76	0.63
5	205.6	0.8 $^{+0.7}_{-0.4}$	99 $^{+213}_{-87}$	1.7 $\pm$ 0.1	112 $\pm$ 55	0.82	0.70

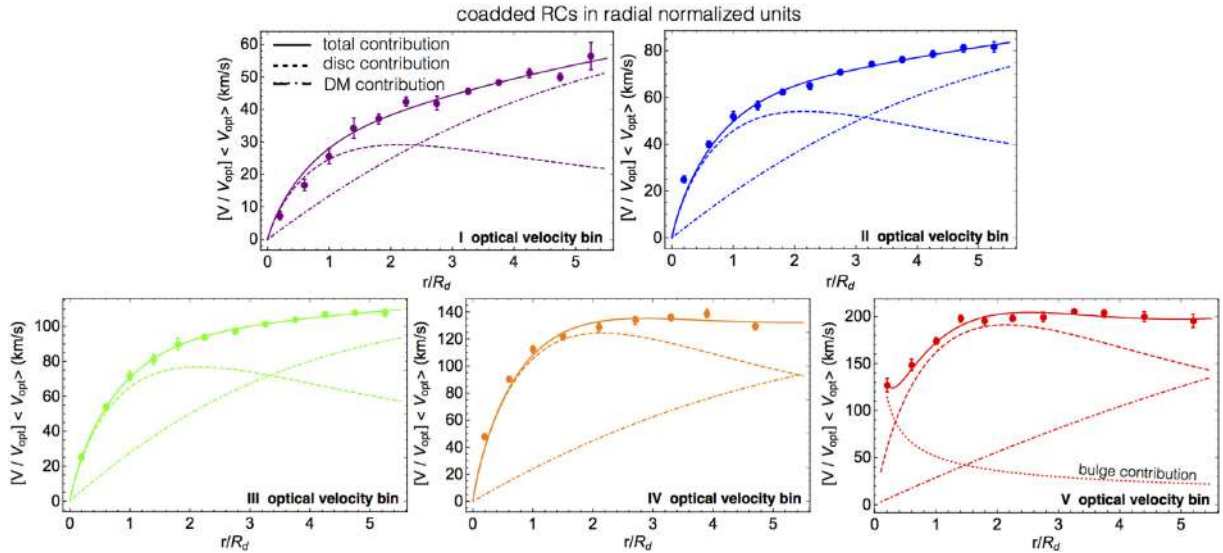


**Figure 7.** In each of the five panels the velocity best-fitting models to the corresponding co-added RCs are shown. The *dashed*, *dot-dashed*, *dotted*, and *solid* lines indicate the stellar disc, the DM halo, the stellar bulge, and the model contribution to the circular velocities.

The errors in the fitting parameter are shown in Table H1 in Appendix H. The relation expressed by equation (9) means that in each galaxy we can evaluate  $R_c$  from its measured  $R_d$ . It is worth noting that a similar relation exists also in normal spirals (Fig. 8).

The second relation we use for the denormalization assumes that for galaxies belonging to each  $V_{\text{opt}}$  bin:

$$\frac{G M_d}{V_{\text{opt}}^2 R_{\text{opt}}} = k, \quad (10)$$

where the  $k$  values are reported in Table 2.  $R_{\text{opt}}$  and  $V_{\text{opt}}$  are measured for all the galaxies, thus equation (10) allows us to evaluate the stellar disc mass  $M_d$  for each of them.

As the third step in the denormalization process we evaluate at  $R_{\text{opt}}$ , for each of the five co-added RCs, the fraction of the baryonic matter:

$$\alpha(R_{\text{opt}}) = \frac{V_d^2(R_{\text{opt}})}{V^2(R_{\text{opt}})}. \quad (11)$$

The  $\alpha(R_{\text{opt}})$  values are reported in Table 2; we assume that all the galaxies included in each optical velocity bin take the same value for  $\alpha(R_{\text{opt}})$ . Then, for each galaxy, we write the DM mass inside the optical radius as:

$$M_{\text{DM}}(R_{\text{opt}}) = [1 - \alpha(R_{\text{opt}})] V_{\text{opt}}^2 R_{\text{opt}} G^{-1}. \quad (12)$$

Finally, by considering equations (6)–(12) together with the result

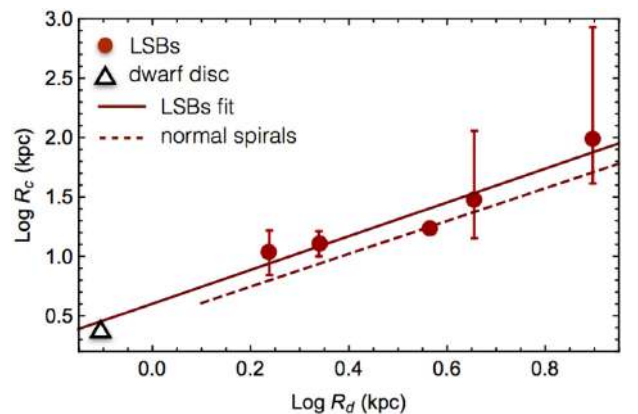


**Figure 8.** Relationship between the DM halo core radius and the stellar disc scale length (*points*) and its best fit (*solid line*) compared to that of the normal spirals (*dashed line*) (e.g. Lapi et al. 2018). The black empty triangle represents the relationship in dwarf disc galaxies (Karukes & Salucci 2017).

from the first denormalization step, we evaluate the central density of the DM halo  $\rho_0$  for each galaxy.

The structural parameters of the dark and luminous matter of the galaxies of our sample, inferred by the denormalization procedure, are reported in Tables G1–G2 in Appendix G. Moreover, we have the basis to infer other relevant quantities of the galaxies structure

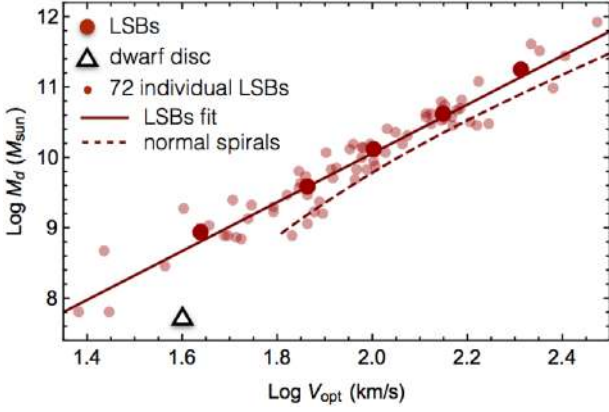


**Figure 9.** Relationship between the stellar disc mass and the optical velocity. The *large points* refer to the values of the five velocity bins, while the *small points* refer to the values of each LSB galaxy. The *solid* and *dashed* lines are the best fit for LSBs and normal spirals (e.g. Lapi et al. 2018). The black triangle represents the dwarf discs (Karukes & Salucci 2017).

that will be involved, in the next section, in building the scaling relations. The virial mass  $M_{\text{vir}}$  that practically encloses the whole mass of a galaxy is evaluated according to:

$$M_{\text{vir}} = \frac{4}{3} \pi 100 \rho_{\text{crit}} R_{\text{vir}}^3, \quad (13)$$

where  $R_{\text{vir}}$  is the virial radius and  $\rho_{\text{crit}} = 9.3 \times 10^{-30} \text{ g cm}^{-3}$  is the critical density of the Universe. The DM central surface density  $\Sigma_0$  is evaluated by the product  $\rho_0$  and  $R_c$ . The  $M_{\text{vir}}$  and  $\Sigma_0$  values for the objects in our sample are shown in Tables G1–G2 in Appendix G.

## 6 THE SCALING RELATIONS

In this section, we work out the scaling relations among the structural properties of dark and luminous matter in each LSB galaxy. Let us stress that for many of the scaling relations we have no a priori insight of how they should be; in this case, the goal is to find a statistically relevant relationship. Then we fit the observational data with the simple power-law model. The errors on the fitting parameters of the various scaling relations and their standard scatters are reported in Table H1 in Appendix H. Hereafter, the masses are expressed in  $M_{\odot}$ , the radial scale length in kpc, the velocities in  $\text{km s}^{-1}$ , and the mass densities in  $\text{g cm}^{-3}$ .

We start with the relation between the stellar disc mass and the optical velocity. Fig. 9 shows that the LSB data are well fitted by

$$\text{Log } M_d = 3.12 + 3.47 \text{ Log } V_{\text{opt}}. \quad (14)$$

This relation holding for the LSBs is similar but not identical to the normal spirals’ one. See the comparison with Lapi et al. (2018) in Fig. 9.

Next, in Fig. 10 (left-hand panel) we show the relation between the DM halo central density and the core radius, which indicates that the highest mass densities are in the smallest galaxies, as also found in normal spirals (Salucci et al. 2007). We find:

$$\text{Log } \rho_0 = -23.15 - 1.16 \text{ Log } R_c. \quad (15)$$

Moreover, we find that the central surface density follows the relationship (see Fig. 10, right-hand panel):

$$\text{Log } \Sigma_0 = \text{Log } (\rho_0 R_c) \simeq 1.9, \quad (16)$$

$\Sigma_0$  is expressed in units of  $M_{\odot}/\text{pc}^2$ .

Remarkably, this relationship extends itself over 18 blue magnitudes and in objects spanning from dwarf to giant galaxies (Spano et al. 2008; Donato et al. 2009; Gentile et al. 2009; Plana et al. 2010; Salucci et al. 2012; Chan 2019; Li et al. 2019).

Then, we consider the baryonic fraction (complementary to the DM fraction) relative to the entire galaxies, namely, the ratio between the stellar mass  $M_* \equiv M_d$  in LSBs and the virial mass  $M_{\text{vir}}$ , that practically represents the whole dark mass of a galaxy. Fig. 11 shows that the lowest fraction of baryonic content is in the smallest galaxies (with the smallest stellar disc mass  $M_d$ ). We note that this ratio increases going towards larger galaxies and then reaches a plateau from which it decreases for the largest galaxies. This finding is in agreement with the inverse ‘U-shape’ of previous works relative to normal spirals (Lapi et al. 2018). Furthermore, our result seems to follow a trend similar to that found in Moster et al. (2010), concerning all Hubble Types.<sup>5</sup> The result points to a less efficient star formation in the smallest LSBs.

Finally, we work out the relationships needed to establish  $V_{\text{URC}}(R; R_{\text{opt}}, V_{\text{opt}})$ , the URC-LSB in physical units (as in Persic et al. 1996). Straightforwardly, we are looking for the universal function  $V_{\text{URC}}(r/R_{\text{opt}}, V_{\text{opt}})$ ,<sup>6</sup> able to reproduce analytically the LSBs RCs in Fig. 1.

This implies that  $M_d$ ,  $R_d$ ,  $R_c$ , and  $\rho_0$  have to be expressed as a function of  $V_{\text{opt}}$ . Thus, we use equation (14) and the following relations, obtained after the denormalization process:

$$\begin{aligned} \text{Log } R_d &= -1.65 + 1.07 \text{ Log } V_{\text{opt}} \\ \text{Log } R_c &= -1.75 + 1.51 \text{ Log } V_{\text{opt}} \\ \text{Log } \rho_0 &= -22.30 - 1.16 \text{ Log } V_{\text{opt}}, \end{aligned} \quad (17)$$

see Fig. 12. We note that the above relations (equations 14–17) show a large scatter, on average  $\sigma \simeq 0.34$  dex, more than three times the value ( $\sigma \simeq 0.1$  dex in Yegorova & Salucci 2007 and Lapi et al. 2018) found in normal spiral galaxies for the respective relations. This poses an issue to the standard procedure (Persic et al. 1996) to build the URC in physical units.

In the previous sections we have found a universal function to reproduce the double-normalized RC of LSBs  $V(r/R_{\text{opt}})/V(R_{\text{opt}})$ . Now we are looking for a universal function to reproduce the RC in physical units  $V(r)$ . In spiral galaxies this is simple since  $M_d$ ,  $R_d$ ,  $R_c$ , and  $\rho_0$  are closely connected.

## 7 THE COMPACTNESS AS THE THIRD PARAMETER IN THE URC

We can reduce the scatter in the LSBs scaling relations and proceed with the URC building by introducing a new parameter: the *compactness* of the stellar mass distribution  $C_*$ . This parameter was first put forward in Karukes & Salucci (2017) to cope with a similar large scatter in the above scaling relations of the *dd* galaxies. In short the large scatter in the previous relationships is due to the fact that galaxies with the same stellar disc mass  $M_d$  (or  $V_{\text{opt}}$ ) can have a very different size for  $R_d$  (i.e.  $\text{Log } R_d$  can vary almost 1 dex). We define this effect with the fact that LSBs have a different ‘stellar compactness’  $C_*$ ; see Figs 2 and 13.

<sup>5</sup>In Moster et al. (2010), the stellar mass  $M_*$  can indicate the mass enclosed in a disc and/or in a bulge.

<sup>6</sup>Hereafter, we express the normalized radial coordinate in terms of the optical radius  $R_{\text{opt}}$ , instead of  $R_d$ , in order to facilitate the comparison with previous works on the URC.

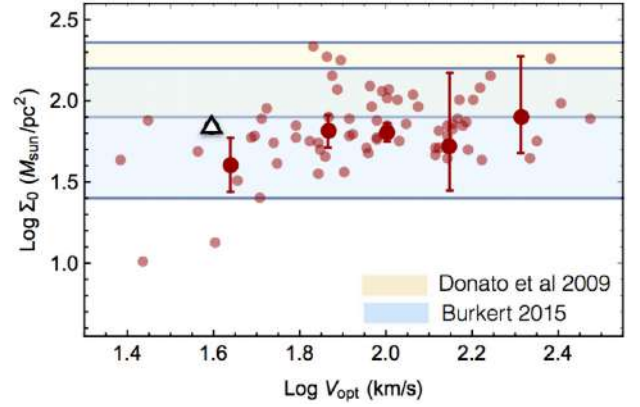
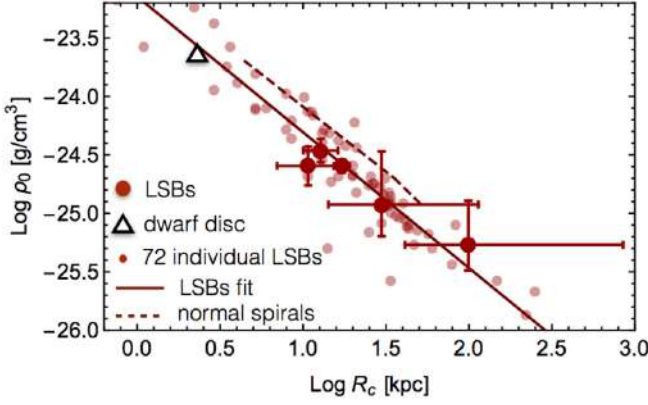


**Figure 10.** Left-hand panel: the relationship between the central DM halo mass density and its core radius. Right-hand panel: surface density  $\Sigma_0 = \rho_0 R_c$  versus their optical velocities  $V_{\text{opt}}$  (LSBs in red points). Also shown is the scaling relation obtained by Donato et al. (2009) (yellow shadowed area) and Burkert (2015) (light blue shadowed area). The black empty triangle represents the dwarf discs (Karukes & Salucci 2017).

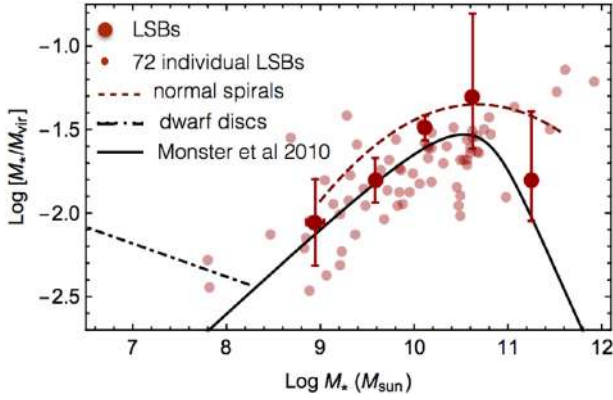


**Figure 11.** Fraction of baryonic matter in LSBs versus their mass in stars (points) compared with that of normal spirals (dashed line) (Lapi et al. 2018), of other Hubble Types (black solid line) (Moster et al. 2010), and of dwarf discs (black dot-dashed line) (Karukes & Salucci 2017).

We define  $C_*$ , starting from the best-fitting linear relation (see Fig. 13):

$$\text{Log } R_d = -3.19 + 0.36 \text{Log } M_d \quad (18)$$

and, according to Karukes & Salucci (2017), we set the stellar compactness through the following relation:

$$C_* = \frac{10^{(-3.19+0.36 \text{Log } M_d)}}{R_d}, \quad (19)$$

where, let us remind,  $R_d$  is measured from photometry. By means of equation (19),  $C_*$  measures, for a galaxy with a fixed  $M_d$ , the deviation between the observed  $R_d$  and the ‘expected’  $R_d$  value from equation (18) (obtained by using the best-fitting line in Fig. 13). In short, at fixed  $M_d$ , galaxies with the smallest  $R_d$  have a high compactness ( $\text{Log } C_* > 0$ ), while galaxies with the largest  $R_d$  have low compactness ( $\text{Log } C_* < 0$ ).

The  $\text{Log } C_*$  values for the galaxies of our sample are shown in Tables G1–G2 in Appendix G and span from  $-0.45$  to  $0.35$ .

By introducing the compactness we reduce the scatter in the relations needed to establish the analytical function of the URC-LSB in physical units. This is highlighted in Fig. 14, where the data

are shown alongside their best-fitting plane.

$$\begin{aligned} \text{Log } M_d &= 2.52 + 3.77 \text{Log } V_{\text{opt}} - 1.49 \text{Log } C_* \\ \text{Log } R_d &= -2.27 + 1.38 \text{Log } V_{\text{opt}} - 1.55 \text{Log } C_* \\ \text{Log } R_c &= -2.62 + 1.96 \text{Log } V_{\text{opt}} - 2.20 \text{Log } C_* \\ \text{Log } \rho_0 &= -20.95 - 1.84 \text{Log } V_{\text{opt}} + 3.38 \text{Log } C_*. \end{aligned} \quad (20)$$

We find that, by using equation (20), the internal scatter of data with respect to the planes is always reduced compared to the case in which  $M_d$ ,  $R_d$ ,  $R_c$ , and  $\rho_0$  were expressed only in terms of  $V_{\text{opt}}$ . The previous average scatter  $\sigma \simeq 0.34$  dex of the 2D relations (equations 14–17), in the 3D relations (equation 20), is reduced to  $\sigma \simeq 0.06$  dex smaller than the typical values obtained for normal spirals.

We now evaluate the analytic expression for the URC (expressed in physical units). By using equation (2) alongside equations (4), (6), and (7) and expressing  $M_d$ ,  $R_d$ ,  $R_c$ , and  $\rho_0$  as in equation (20), we obtain:

$$\begin{aligned} V^2(x, V_{\text{opt}}, C_*) &= 2.2 x^2 \times 10^{f_1(V_{\text{opt}}, C_*)} \\ &\times [I_0 K_0 - I_1 K_1] + 1.25/x \times 10^{f_2(V_{\text{opt}}, C_*)} \\ &\times \{-t g^{-1}[3.2 x \times 10^{f_3(V_{\text{opt}}, C_*)}]\} \\ &+ \ln[1 + 3.2 x \times 10^{f_3(V_{\text{opt}}, C_*)}] \\ &+ 0.5 \ln[1 + 10.24 x^2 \times 10^{2 f_3(V_{\text{opt}}, C_*)}], \end{aligned} \quad (21)$$

where  $I_n$ ,  $K_n$  are the modified Bessel functions evaluated at  $1.6x$ , with  $x = r/R_{\text{opt}}$  and

$$\begin{aligned} f_1(V_{\text{opt}}, C_*) &= 9.79 + 2.39 \text{Log } V_{\text{opt}} + 0.05 \text{Log } C_* \\ f_2(V_{\text{opt}}, C_*) &= -0.55 + 2.65 \text{Log } V_{\text{opt}} - 1.67 \text{Log } C_* \\ f_3(V_{\text{opt}}, C_*) &= 0.35 - 0.58 \text{Log } V_{\text{opt}} + 0.65 \text{Log } C_*. \end{aligned} \quad (22)$$

Finally, we plot in Fig. 15 the URC (equations 21–22) considering  $\text{Log } C_* = 0$ , corresponding to the case in which all the LSBs data in Fig. 13 were lying on the regression line (or, analogously, the case in which the spread of LSBs data in Fig. 2 was small). The curve shown in Fig. 15 is in good agreement with the LSBs RCs data. On average, the uncertainty between the velocity data and the URC velocity predicted values is  $\Delta V/V \simeq 19$  per cent, which can be reduced to  $\Delta V/V \simeq 8$  per cent, when the observational errors, the systematics, the small non-circularities, and the prominent bulge

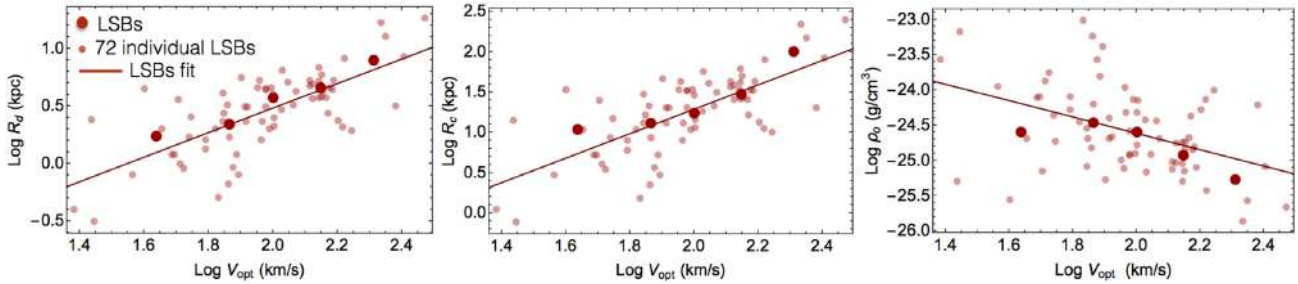


**Figure 12.** LSBs relationships between (a) the stellar disc scale length, (b) the DM core radius, and (c) the central DM core density versus the optical velocity (first, second, and third panel).

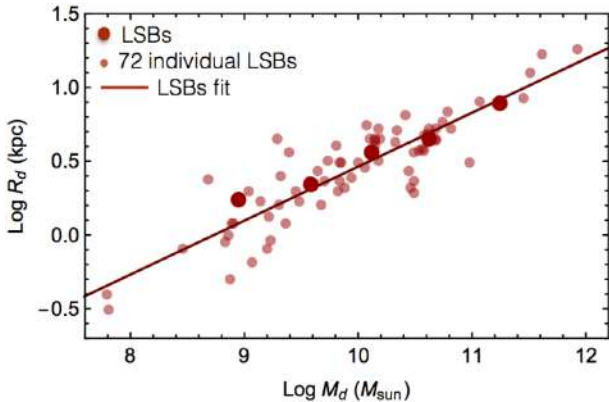


**Figure 13.** Relationship between the stellar disc scale length and the stellar disc mass.

component<sup>7</sup> (as in ESO534–G020) are taken into account in the individual RCs. This result, approximately equal to that found in normal spirals (Persic et al. 1996), highlights the success of the URC method also in LSBs galaxies. The smallness of the uncertainty achieved in the URC-LSB (physical) is evident in Appendix I, where the individual RCs are tested. As a gauge we point out that F583-4, NGC 4395, UGC5005, F568V1, ESO444–G074 have a value of  $\Delta V/V \simeq 8$  per cent. Moreover, in Appendix I, the individual RCs are tested by assuming (i)  $\text{Log } C_* = 0$  and (ii) their values of  $C_*$  (reported in Tables G1–G2 in Appendix G).

Finally, in Fig. 16 we show the URC obtained with three significant different values of stellar compactness. The central yellow surface has  $\text{Log } C_* = 0.00$  (standard case) and the other two surfaces have  $\text{Log } C_* = -0.45$  (the minimum value achieved in the LSB sample) and  $\text{Log } C_* = +0.35$  (the maximum one). The three surfaces appear similar, however when we normalize them with respect to  $V_{\text{opt}}$  along the velocity axis, their profiles appear different, see Fig. 17. Nevertheless, the differences between the URC with  $\text{Log } C_* = 0.00$  and the URC with the appropriate values of  $C_*$  for each individual object lie within the URC error bars for most of the objects (see Appendix I).

### 7.1 The relevance of $C_*$ in LSB galaxies

Completing our analysis, we have discovered the relevance of  $C_*$  in the LSB galaxies. By resuming, this work shows that:

(i) the compactness is linked to the spread in the  $V_{\text{opt}}-R_d$  plot (Fig. 2). Galaxies at fixed  $V_{\text{opt}}$  can have smaller  $R_d$  (higher  $C_*$ ) or larger  $R_d$  (lower  $C_*$ ) than the average. The range of  $\text{Log } R_d$  at fixed  $V_{\text{opt}}$  can reach almost 1 dex;

(ii) the profiles of the various RCs can be affected by the compactness (see e.g. Fig. 17). Thus, the spread in the profiles of the RCs in each velocity bin (see Figs 4–5) is not only due to the large width of the optical velocity bins,<sup>8</sup> but it is also due to the different values of the galaxies compactness.

(iii) the compactness is the main source for the large scatter ( $\sigma \simeq 0.34$ ) in the 2D scaling relations (see Figs 9–14).

Taking all this into account, we point out that in the URC-LSB building procedure, having an improved statistic, the optimal approach would be considering from the start to bin the available RCs in  $C_*$  (obtained by the spread of data in the  $V_{\text{opt}}-R_d$  plot in Fig. 2) contemporaneously to  $V_{\text{opt}}$ . Moreover, with a sufficiently higher statistics, we can also increase the number of the velocity bins and characterize each of them with a smaller  $V_{\text{opt}}$  range to reach the performance of Persic et al. (1996).

Finally, we stress that in the LSBs there is no one-to-one correspondence among the optical velocity, the optical radius, the luminosity, the virial mass, and other galaxies quantities. Then, if we order the RCs normalized in radial units, according to quantities different from the optical velocity (as in Fig. 1), they would not lie on a unique surface but, according to the spread of the stellar compactness among the objects, will give rise to a spread of RC data lying on different surfaces.

## 8 THE CORRELATION BETWEEN THE COMPACTNESS OF THE STELLAR AND THE DM MASS DISTRIBUTIONS

Following Karukes & Salucci (2017), we evaluate also the compactness of the DM halo  $C_{\text{DM}}$ , i.e. we investigate the case in which the galaxies with the same virial (dark) mass  $M_{\text{vir}}$  exhibit different core radius  $R_c$ .

The  $M_{\text{vir}}$  versus  $R_c$  relationship is shown in Fig. 18 alongside the best-fitting linear relation, described by

$$\text{Log } R_c = -5.32 + 0.56 \text{Log } M_{\text{vir}}. \quad (23)$$

<sup>7</sup>The bulge component is taken into account in the co-added RCs modelling, but not in the final URC, going beyond the scope of the paper.

<sup>8</sup>Given the limited number of available RCs, each optical velocity bin includes galaxies with a certain range in  $V_{\text{opt}}$ , causing the corresponding RCs to have (moderately) different profiles, analogously to normal spirals.

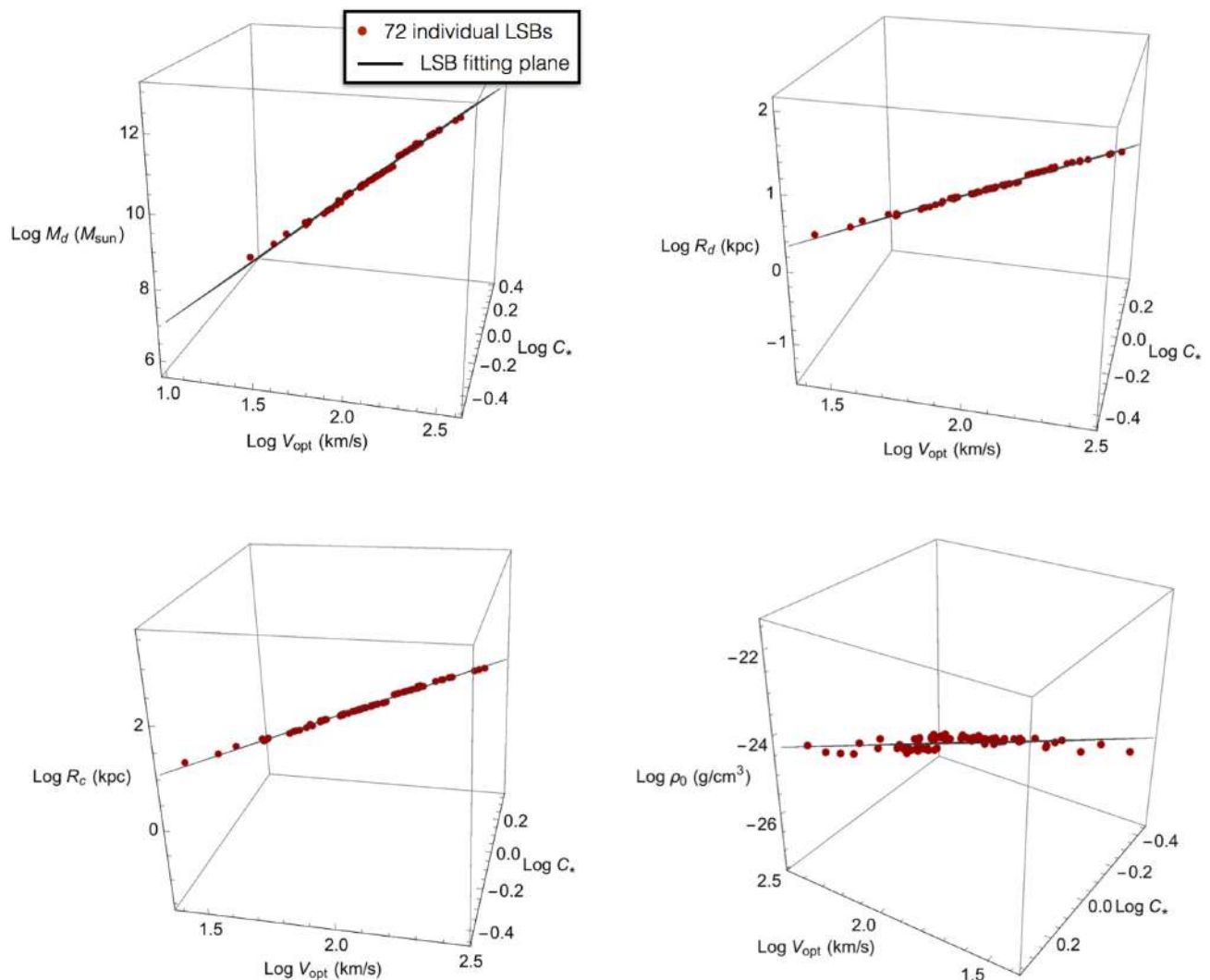


**Figure 14.** In the panels we show the relationships between (a) the stellar disc mass, (b) the stellar disc scale length, (c) the DM core radius, and (d) the central DM core density versus the optical velocity and the compactness of the stellar distribution. The errors in the distance of galaxies, which propagates on  $R_c$ ,  $M_d$ ,  $R_d$ ,  $\rho_0$ , are negligible in the above for 3D relationships.

Then, according to Karukes & Salucci (2017), we define the compactness  $C_{DM}$  of the DM halo as:

$$C_{DM} = \frac{10^{(-5.32+0.56 \text{Log } M_{vir})}}{R_c}. \quad (24)$$

Thus, at fixed  $M_{vir}$ , galaxies with smaller  $R_c$  have higher compactness ( $\text{Log } C_{DM} > 0$ ), while galaxies with larger  $R_c$  have lower compactness ( $\text{Log } C_{DM} < 0$ ).

The values obtained for  $\text{Log } C_{DM}$  are reported in Tables G1–G2 in Appendix G and span from  $-0.57$  to  $0.30$ .

Then, we plot the compactness of the stellar disc versus the compactness of the DM halo in Fig. 19. We note that  $C_*$  and  $C_{DM}$  are strictly related: galaxies with high  $C_*$ , also have high  $C_{DM}$ . The logarithmic data are well fitted by the linear relation:

$$\text{Log } C_* = 0.00 + 0.90 \text{Log } C_{DM}. \quad (25)$$

The results are in very good agreement with those obtained for *dd* galaxies (Karukes & Salucci 2017), whose best-fitting relation is given by  $\text{Log } C_* = 0.77 \text{Log } C_{DM} + 0.03$ . In the figure we realize

that the average difference between the two relationship is just about 0.1 dex.

This result is remarkable because the same relation is found for two very different types of galaxies (LSBs and *dds*). The strong relationship between the two compactness certainly indicates that the stellar and the DM distributions follow each other very closely. In a speculative way, given the very different distribution of luminous matter in an exponential thin disc and the distribution of DM in a spherical cored halo, such strong correlation in equation (25) might point to a non-standard interaction between the baryonic and the DM, a velocity-dependent self-interaction in the dark sector, or a fine-tuned baryonic feedback (e.g. Di Cintio et al. 2014; Chan et al. 2015).

## 9 CONCLUSIONS

We analysed a sample of 72 LSB galaxies selected from literature, whose optical velocities  $V_{opt}$  span from  $\sim 24$  to  $\sim 300 \text{ km s}^{-1}$ . Their RCs, normalized in the radial coordinate with respect to the stellar disc scale length  $R_d$  (or the optical radius  $R_{opt}$ ) and ordered according

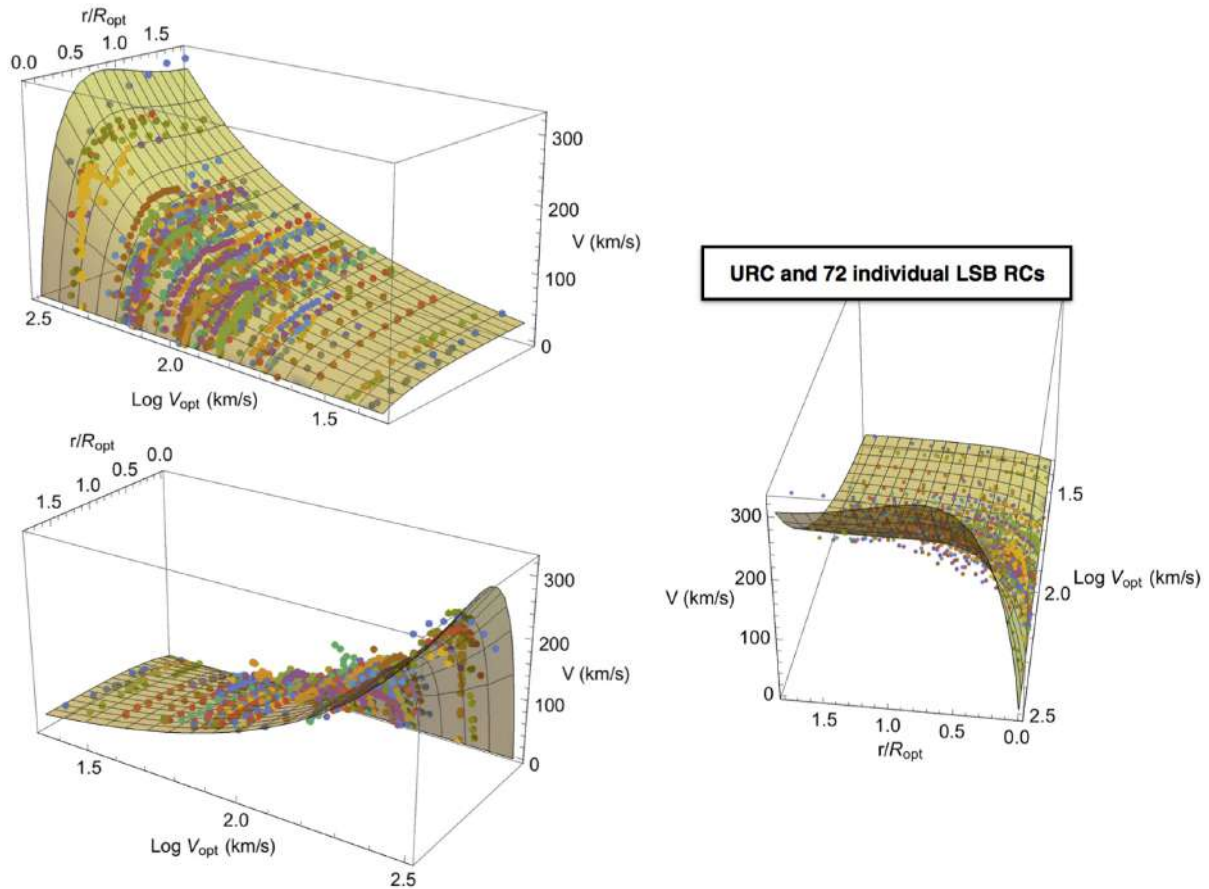


**Figure 15.** LSBs URC, with compactness  $\text{Log } C_* = 0$ , and the individual 72 LSBs RCs.

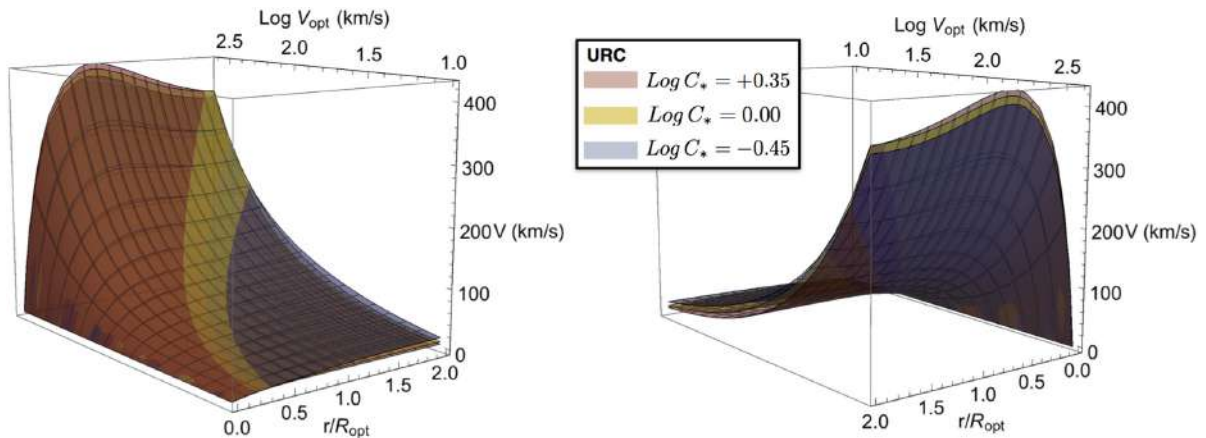


**Figure 16.** URC in physical velocity units for three different values of stellar compactness: low ( $\text{Log } C_* = -0.45$ ), standard ( $\text{Log } C_* = 0.00$ ), and high ( $\text{Log } C_* = +0.35$ ) stellar compactness, respectively, in *blue*, *yellow*, and *red* colours. The figure in the second panel corresponds to that of the first panel when rotated by  $180^\circ$  around the velocity axis.

to the increasing optical velocity  $V_{\text{opt}}$ , follow a universal trend (Fig. 1), analogously to the normal (HSB) spirals. This led us to build the URC of LSBs as in Persic et al. (1996), i.e. to find an analytic expression to reproduce any circular velocity by means of only few observable parameters (e.g.  $R_{\text{opt}}$  and  $V_{\text{opt}}$ ).

The building of the URC allows us to obtain the properties of the stellar and DM distribution and to evaluate the scaling relations valid for the whole population of objects. The analysis on the LSBs

RCs leads us to a scenario which is very similar qualitatively, but not quantitatively, to that of the normal spirals. In detail, in both cases, we observe that the main contribution to the circular velocity, in the innermost galactic region, is given by the stellar disc component, while, in the external region it is given by a cored DM spherical halo. Moreover, the fraction of DM that contributes to the RCs is more relevant as lower  $V_{\text{opt}}$  is, i.e. in smaller galaxies (Fig. 7).

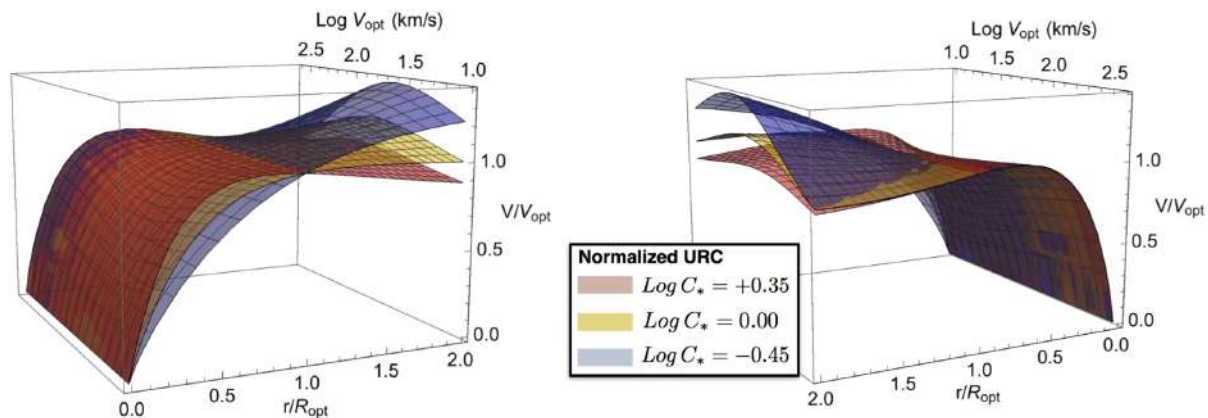


**Figure 17.** URC in double-normalized units for three values of the stellar compactness:  $\text{Log } C_* = -0.45, 0.00, +0.35$ , respectively, in blue, yellow, and red colours. Notice that the figure in the second panel corresponds to that of the first panel rotated of  $180^\circ$  around the velocity axis.

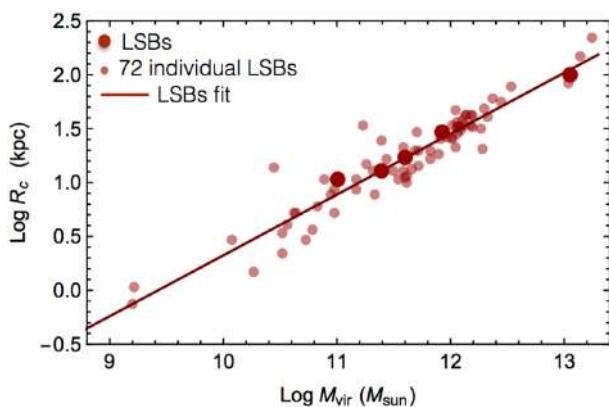


**Figure 18.** Relationship between the DM halo core radius and the virial mass.

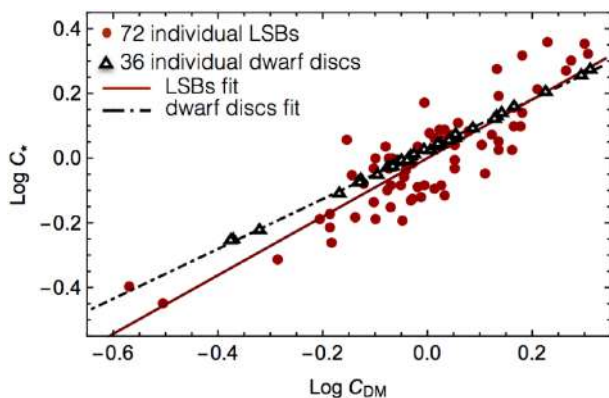


**Figure 19.** Relationship between the compactness of the stellar disc and the compactness of the DM halo (red points). The black triangles refer to the dwarf discs of Karukes & Salucci (2017). The solid and the dot-dashed lines are the best-fitting relations for LSBs and dwarf discs.

The scaling relations among the galactic properties seem to follow a similar trend in LSB galaxies and HSB spirals (Figs 8–10).

On the other side, there is a clear difference: we realize the presence of a large scatter in the LSBs relationships with respect to that found in normal spirals (see Lapi et al. 2018). Such difference can be traced back to the large spread of the  $V_{\text{opt}}-R_d$  data (see Fig. 2) or, analogously, to the large spread of the  $R_d-M_d$  relationship

in Fig. 13. This finding leads us to introduce the concept of *compactness* of the luminous matter distribution  $C_*$ , involved for the first time in Karukes & Salucci (2017) to cope with a similar issue in the case of *dd* galaxies.

We have that in galaxies with a fixed value for  $M_d$ , the smaller the  $R_d$ , the higher the  $C_*$ . By considering  $C_*$  in the scaling relations, the scatter is much reduced (it becomes smaller than that of the normal spirals). By involving this new parameter, we proceed with the building of the analytic universal expression to describe all the LSBs RCs (in physical units,  $\text{km s}^{-1}$  versus kpc). The resulting URC,  $V(r; R_{\text{opt}}, V_{\text{opt}}, C_*)$  in equations (21)–(22), well describes all the RCs of our sample (Figs 15 and 11–15). The average scatter of the RCs data from the fitting surface in Fig. 15 achieves the small value of  $\Delta V/V \simeq 0.08$ , taking into account the observational errors, the systematics, and the small non-circularities in the motion. This result remarks the success of the method leading to the URC and of the relevance of  $C_*$  in the RCs profiles (Fig. 17) and in the scaling relations, which has been discovered in building the URC.

With larger statistics, one should subdivide the RCs according to the galaxies  $C_*$  and  $V_{\text{opt}}$ .

An important finding concerns the compactness of the DM distribution  $C_{\text{DM}}$ , indicating galaxies with the same virial mass and different core radius (Fig. 18). We find a strong correlation between  $C_*$  and  $C_{\text{DM}}$  as also found in Karukes & Salucci (2017) (Fig 19): *the distributions of stellar disc and of its enveloping DM halo are entangled*. In a speculative way, this finding appears to be of very important relevance for the nature of DM. In fact, the strong correlation between  $C_*$  and  $C_{\text{DM}}$  may hint to the existence of non-standard interactions between the luminous matter and the DM, or non-trivial self-interaction in the DM sector or a (hugely) fine-tuned baryonic feedback on the collisionless DM distribution.

Finally, the LSBs URC provides us with the best observational data to test specific density profiles (e.g. NFW, WDM, Fuzzy DM) or alternatives to DM (e.g. MOND). The normal spirals' URC, in connection with the normal spirals'  $R_{\text{opt}}$  versus  $V_{\text{opt}}$  relationship, is a function of  $V_{\text{opt}}$ :  $V_{\text{URC(ns)}}(r/R_{\text{opt}}, V_{\text{opt}})$  (*ns* stands for normal spirals). Therefore, to represent *all* the normal spirals' individual RCs it is sufficient to evaluate  $V_{\text{URC(ns)}}(r/R_{\text{opt}}, V_{\text{opt}})$  for a reasonable number  $j$  of  $V_{\text{opt}}$  values, homogeneously spread in the spirals  $V_{\text{opt}}$  range. Any mass model under test must reproduce the  $V_{\text{opt}}$ -dependent URC. Instead, the LSBs URC, in connection with the LSBs  $R_{\text{opt}}$  versus  $V_{\text{opt}}$  and  $C_*$  relationship, is a function of *two* galaxy structural properties:  $V_{\text{opt}}$  and  $C_*$ . In this case, to represent *all* the LSBs RCs we have to build  $V_{\text{URC(LSB)}}(r/R_{\text{opt}}, V_{\text{opt}}, C_*)$ . We need a large sample of RCs

of galaxies of different  $V_{\text{opt}}$  and  $C_*$  yielding a reasonable number of RCs in each of the more numerous ( $V_{\text{opt}}$ ;  $C_*$ ) bins we have to employ. The galaxies model under test must reproduce a much complex (observational driven) URC than that of normal spirals which depends on just the structural parameter  $V_{\text{opt}}$ .

## ACKNOWLEDGEMENTS

We thank E. Karukes and A. Lapi for useful discussions. We thank Brigitte Greinoecker for improving the text. We thank the referee for her/his several inputs that have improved the paper.

## REFERENCES

- Bell E. F., Barnaby D., Bower R. G., de Jong R. S., Harper D. A., Hereld M., Loewenstein R. F., Rauscher B. J., 2000, *MNRAS*, 312, 470
- Bothun G. D., Schombert J. M., Impey C. D., Sprayberry D., McGaugh S. S., 1993, *AJ*, 106, 530
- Boylan-Kolchin M., Bullock J. S., Kaplinghat M., 2012, *MNRAS*, 422, 1203
- Bullock J. S., Boylan-Kolchin M., 2017, *ARA&A*, 55, 343
- Burkert A., 1995, *ApJ*, 447, L25
- Burkert A., 2015, *ApJ*, 808, 158
- Carignan C., Puche D., 1990, *AJ*, 100, 641C
- Catinella B., Giovanelli R., Haynes M. P., 2006, *ApJ*, 640, 751
- Chan M., 2019, *Sci. Rep.*, 9, 3570
- Chan T. K., Keref D., Oñorbe J., Hopkins P. F., Muratov A. L., Faucher-Giguère C.-A., Quataert E., 2015, *MNRAS*, 454, 2981
- Das M., 2013, *J. Astrophys. Astron.*, 34, 19
- de Blok W. J. G., van der Hulst J., Bothun G., 1995, *MNRAS*, 274, 235
- de Blok W. J. G., Bosma A., 2002, *A&A*, 385, 816
- de Blok W. J. G., McGaugh S. S., 1997, *MNRAS*, 290, 533
- de Blok W. J. G., McGaugh S. S., van der Hulst J. M., 1996, *MNRAS*, 283, 18
- de Blok W. J. G., McGaugh S. S., Rubin V. C., 2001, *AJ*, 122, 2381
- de Vega H. J., Moreno O., Moya de Guerra E., Ramón Medrano M., Sánchez N. G., 2013, *Nucl. Phys. B.*, 866, 177
- Del Popolo A., Kroupa P., 2009, *A&A*, 502, 733
- Di Cintio A., Brook C. B., Macciò A. V., Stinson G. S., Knebe A., Dutton A. A., Wadsley J., 2014, *MNRAS*, 437, 415
- Donato F. et al., 2009, *MNRAS*, 397, 1169
- Elbert O. D., Bullock J. S., Garrison-Kimmel S., Rocha M., Oñorbe J., Peter A. H. G., 2015, *MNRAS*, 453, 29
- Evoli C., Salucci P., Lapi A., Danese L., 2011, *ApJ*, 743, 45
- Faber S. M., Gallagher J. S., 1979, *ARA&A*, 17, 135
- Ferrero I., Abadi M. G., Navarro J. F., Sales L. V., Gurovich S., 2012, *MNRAS*, 425, 2817
- Freeman K. C., 1970, *ApJ*, 160, 811
- Garrison-Kimmel S., Boylan-Kolchin M., Bullock J. S., Kirby E. N., 2014, *MNRAS*, 444, 222
- Gentile G., Salucci P., Klein U., Vergani D., Kalberla P., 2004, *MNRAS*, 351, 903
- Gentile G., Burkert A., Salucci P., Klein U., Walter F., 2005, *ApJ*, 634, L145
- Gentile G., Famaey B., Zhao H., Salucci P., 2009, *Nature*, 461, 627
- Karukes E. V., Salucci P., 2017, *MNRAS*, 465, 4703
- Klypin A., Kravtsov A. V., Valenzuela O., Prada F., 1999, *ApJ*, 522, 82
- Klypin A., Karachentsev I., Makarov D., Nasonova O., 2015, *MNRAS*, 454, 1798
- Kolb E. W., Turner M. S., 1990, *The Early Universe*. Addison Wesley, Redwood City, CA
- Kuzio de Naray R., McGaugh S. S., de Blok W. J. G., Bosma A., 2006, *ApJS*, 165, 461
- Kuzio de Naray R., McGaugh S. S., de Blok W. J. G., 2008, *ApJ*, 676, 920
- Lapi A., Salucci P., Danese L., 2018, *ApJ*, 859, 2
- Li P., Lelli F., McGaugh S. S., Starkman N., Schombert J. M., 2019, *MNRAS*, 482, 5106
- López Fune E., 2018, *MNRAS*, 475, 2132
- Lovell M. R., Frenk C. S., Eke V. R., Jenkins A., Gao L., Theuns T., 2014, *MNRAS*, 439, 300
- Marchesini D., D'Onghia E., Chincarini G., Firmani C., Conconi P., Molinari E., Zacchei A., 2002, *ApJ*, 575, 801
- Mashchenko S., Couchman H. M. P., Wadsley J., 2006, *Nature*, 442, 539
- McGaugh S. S., 1994, *ApJ*, 426, 135
- Memola E., Salucci P., Babić A., 2011, *A&A*, 534, A50
- Moore B., Ghigna S., Governato F., Lake G., Quinn T., Stadel J., Tozzi P., 1999, *ApJ*, 524, L19
- Morelli L., Corsini E. M., Pizzella A., Dalla Bontà E., Coccato L., Méndez-Abreu J., Cesetti M., 2012, *MNRAS*, 423, 962
- Moster B., Somerville R., Maubetsch C., van den Bosch F., Macciò A., Naab N., Oser L., 2010, *ApJ*, 710, 903
- Navarro J. F., Eke V. R., Frenk C. S., 1996, *MNRAS*, 283, L72
- Noordermeer E., van der Hulst J. M., Sancisi R., Swaters R. S., van Albada I. T. S., 2007, *MNRAS*, 376, 1513
- Oh S.-H., de Blok W. J. G., Brinks E., Walter F., Kennicutt J. R. C., 2011, *AJ*, 141, 193
- Palunas P., Williams T. B., 2000, *AJ*, 120, 2884
- Papastergis E., Martin A. M., Giovanelli R., Haynes M. P., 2011, *ApJ*, 739, 38
- Papastergis E., Giovanelli R., Haynes M. P., Shankar F., 2015, *A&A*, 574, A113
- Persic M., Salucci P., 1991, *ApJ*, 368, 60
- Persic M., Salucci P., Stel F., 1996, *MNRAS*, 281, 27
- Pickering T. E., Impey C. D., van Gorkom J. H., Bothun G. D., 1997, *AJ*, 114, 1858
- Pickering T. E., van Gorkom J. H., Impey C. D., Quillen A. C., 1999, *AJ*, 118, 765
- Pizzella A., Corsini E. M., Sarzi M., Magorrian J., Méndez-Abreu J., Coccato L., Morelli L., Bertola F., 2008, *MNRAS*, 387, 1099
- Plana H., Amram P., Mendes de Oliveira C., Balkowski C., 2010, *AJ*, 139, 1
- Pontzen A., Governato F., 2014, *Nature*, 506, 171
- Read J. I., Gilmore G., 2005, *MNRAS*, 356, 107
- Rhee M. H., 1996, PhD thesis, Univ. Groningen
- Roscoe D. F., 1999, *Pramana*, 53, 1033
- Rosenbaum S. D., Bomans D. J., 2004, *A&A*, 422, L5
- Rubin V. C., Burstein D., Ford J. W. K., Thonnard N., 1985, *ApJ*, 289, 81
- Salucci P., 2001, *MNRAS*, 320, L1
- Salucci P., Martins C. F., Lapi A., 2010, <http://www.sissa.it/ap/dmg/dmaw/presentation.html>
- Salucci P., 2019, *A&AR*, 27, 2
- Salucci P., Burkert A., 2000, *ApJ*, 537, L9
- Salucci P., Lapi A., Tonini C., Gentile G., Yegorova I., Klein U., 2007, *MNRAS*, 378, 41
- Salucci P., Wilkinson M. I., Walker M. G., Gilmore G. F., Grebel E. K., Koch A., Frigerio Martins C., Wyse R. F. G., 2012, *MNRAS*, 420, 2034
- Simon J. D., Bolatto A. D., Leroy A., Blitz L., Gates E. L., 2005, *ApJ*, 621, 757
- Spano M., Marcelin M., Amram P., Carignan C., Epinat B., Hernandez O., 2008, *MNRAS*, 383, 297
- Swaters R. A., Madore B. F., Trewheella M., 2000, *ApJ*, 531, L107
- Swaters R. A., Madore B. F., van den Bosch F. C., Balcells M., 2003, *ApJ*, 583, 732
- van Zee L., Haynes M. P., Salzer J. J., Broeils A. H., 1997, *AJ*, 113, 1618
- van den Bosch F. C., Swaters R. A., 2001, *MNRAS*, 325, 1017
- van der Hulst J. M., Skillman E. D., Smith T. R., Bothun G. D., McGaugh S. S., de Blok W. J. G., 1993, *AJ*, 106, 548
- Vogelsberger M., Zavala J., Simpson C., Jenkins A., 2014, *MNRAS*, 444, 3684
- Weinberg D. H., Bullock J. S., Governato F., Kuzio de Naray R., Peter A. H. G., 2015, *Proc. Natl. Acad. Sci.*, 112, 12249
- Yegorova I. A., Salucci P., 2007, *MNRAS*, 377, 507
- Zavala J., Jing Y. P., Faltenbacher A., Yepes G., Hoffman Y., Gottlöber S., Catinella B., 2009, *ApJ*, 700, 1779
- Zwaan M. A., van der Hulst J. M., de Blok W. J. G., McGaugh S. S., 1995, *MNRAS*, 273, L35

**SUPPORTING INFORMATION**

Supplementary data are available at [MNRAS](https://www.mnras.org/) online.

**LSBdata.txt**

Please note: Oxford University Press is not responsible for the content or functionality of any supporting materials supplied by the authors. Any queries (other than missing material) should be directed to the corresponding author for the article.

**APPENDIX A: UNIVERSALITY IN NORMAL SPIRALS**

Fig. A1, from Persic et al. (1996) and Catinella et al. (2006), allows us to appreciate the *universality* of the RCs in normal spirals after the radial normalization. Let us point out the trend of the RCs from small to large galaxies.

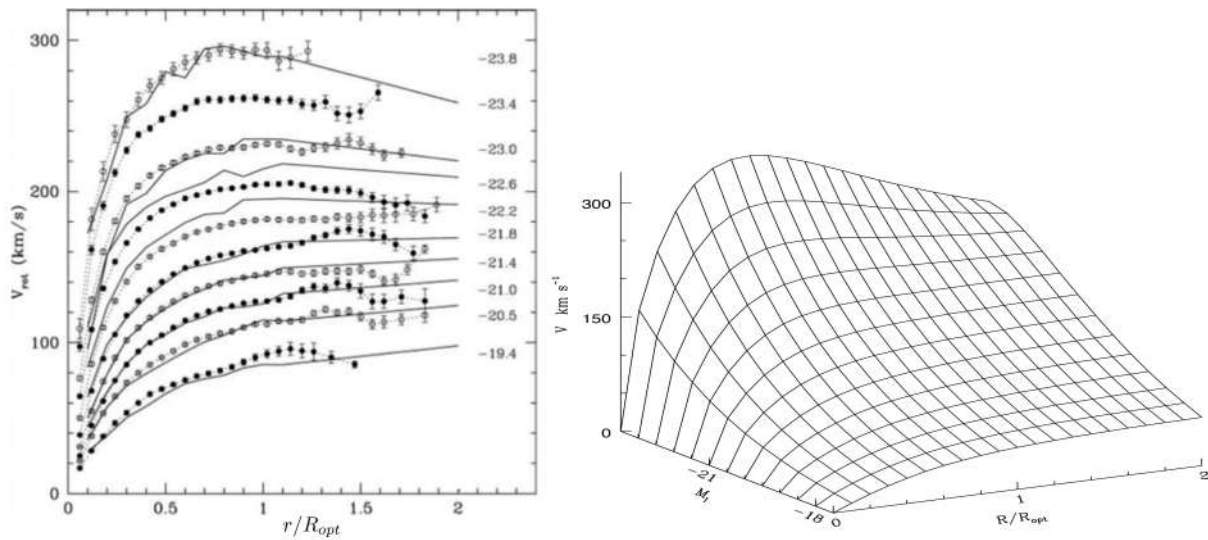


**Figure A1.** Top panel: co-added RCs from 3100 normal spirals, obtained by plotting together the results by Persic et al. (1996) and Catinella et al. (2006) (originally in the slides by Salucci 2010). Also indicated are the absolute I-magnitudes. Bottom panel: URC (Persic et al. 1996).

**APPENDIX B: LSB GALAXIES SAMPLE AND REFERENCES**

In Table B1, we report the list of the LSB galaxies of this work with their related references.

**APPENDIX C: ROTATION CURVES IN PHYSICAL UNITS**

In Fig. C1, the 72 LSB RCs are shown in physical units. Here, all the data are included, while the first panel of Fig. 3 includes only data with  $r \leq 30$  kpc.

**Table B1.** LSB sample: galaxy names and references of their RCs and photometric data. Note that some galaxies have multiple RC data.

Galaxy	Reference	Galaxy	Reference
NGC 100	de Blok & Bosma (2002)	UGC 11557	Swaters et al. (2003)
NGC 247	Carignan & Puche (1990)	UGC 11583	de Blok et al. (2001)
NGC 959	Kuzio de Naray et al. (2008)	UGC 11616	de Blok et al. (2001)
NGC 2552	Kuzio de Naray et al. (2008)	UGC 11648	de Blok et al. (2001)
NGC 2552	de Blok & Bosma (2002)	UGC 11748	de Blok et al. (2001)
NGC 2552	Swaters et al. (2003)	UGC 11819	de Blok et al. (2001)
NGC 2552	van den Bosch & Swaters (2001)	ESO 186–G055	Pizzella et al. (2008)
NGC 3274	de Blok & Bosma (2002)	ESO 206–G014	Pizzella et al. (2008)
NGC 3274	Swaters et al. (2003)	ESO 215–G039	Palunas & Williams (2000)
NGC 3347B	Palunas & Williams (2000)	ESO 234–G013	Pizzella et al. (2008)
NGC 4395	de Blok & Bosma (2002)	ESO 268–G044	Palunas & Williams (2000)
NGC 4395	van den Bosch & Swaters (2001)	ESO 322–G019	Palunas & Williams (2000)
NGC 4455	de Blok & Bosma (2002)	ESO 323–G042	Palunas & Williams (2000)
NGC 4455	Marchesini et al. (2002)	ESO 323–G073	Palunas & Williams (2000)
NGC 4455	van den Bosch & Swaters (2001)	ESO 374–G003	Palunas & Williams (2000)
NGC 5023	de Blok & Bosma (2002)	ESO 382–G006	Palunas & Williams (2000)
NGC 5204	Swaters et al. (2003)	ESO 400–G037	Pizzella et al. (2008)
NGC 5204	van den Bosch & Swaters (2001)	ESO 444–G021	Palunas & Williams (2000)
NGC 7589	Pickering et al. (1997)	ESO 444–G047	Palunas & Williams (2000)
UGC 628	de Blok & Bosma (2002)	ESO 488–G049	Pizzella et al. (2008)
UGC 634	van Zee et al. (1997)	ESO 509–G091	Palunas & Williams (2000)
UGC 731	de Blok & Bosma (2002)	ESO 534–G020	Pizzella et al. (2008)
UGC 731	Swaters et al. (2003)	F561-1	de Blok et al. (1996)
UGC 731	van den Bosch & Swaters (2001)	F563-V1	de Blok et al. (1996)
UGC 1230	de Blok & Bosma (2002)	F563-V2	Kuzio de Naray et al. (2006)
UGC 1230	van der Hulst et al. (1993)	F563-V2	de Blok et al. (1996)
UGC 1281	Kuzio de Naray et al. (2006)	F565-V2	de Blok et al. (1996)
UGC 1281	de Blok & Bosma (2002)	F568-1	Swaters, Madore & Trewhella (2000)
UGC 1551	Kuzio de Naray et al. (2008)	F568-3	Kuzio de Naray et al. (2006)
UGC 2684	van Zee et al. (1997)	F568-3	de Blok et al. (2001)
UGC 2936	Pickering et al. (1999)	F568-3	Swaters et al. (2000)
UGC 3137	de Blok & Bosma (2002)	F568-6	Pickering et al. (1997)
UGC 3174	van Zee et al. (1997)	F568-V1	Swaters et al. (2000)
UGC 3371	de Blok & Bosma (2002)	F571-8	Marchesini et al. (2002)
UGC 3371	van den Bosch & Swaters (2001)	F571-8	de Blok et al. (2001)
UGC 4115	de Blok et al. (2001)	F571-V1	de Blok et al. (1996)
UGC 4278	de Blok & Bosma (2002)	F574-1	Swaters et al. (2000)
UGC 5005	de Blok & McGaugh (1997)	F574-2	de Blok et al. (1996)
UGC 5272	Kuzio de Naray et al. (2008)	F579-V1	de Blok et al. (2001)
UGC 5272	de Blok & Bosma (2002)	F583-1	Kuzio de Naray et al. (2008)
UGC 5716	van Zee et al. (1997)	F583-1	Marchesini et al. (2002)
UGC 5750	Kuzio de Naray et al. (2006)	F583-1	de Blok et al. (2001)
UGC 5750	de Blok & Bosma (2002)	F583-1	de Blok et al. (1996)
UGC 5999	van der Hulst et al. (1993)	F583-4	Kuzio de Naray et al. (2006)
UGC 7178	van Zee et al. (1997)	F583-4	de Blok et al. (2001)
UGC 8837	de Blok & Bosma (2002)	F730-V1	de Blok et al. (2001)
UGC 9211	van den Bosch & Swaters (2001)	PGC 37759	Morelli et al. (2012)
UGC 11454	de Blok et al. (2001)		

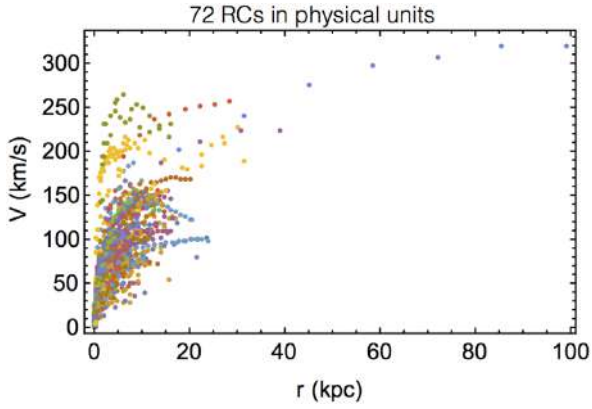


Figure C1. The 72 LSB RCs in physical units (all data).

### APPENDIX D: ROTATION CURVES IN VELOCITY BINS

In Fig. D1 we show the LSBs RCs separately in the five velocity bins, both in physical units and in double-normalized units (i.e. along the radial and the velocity axes).

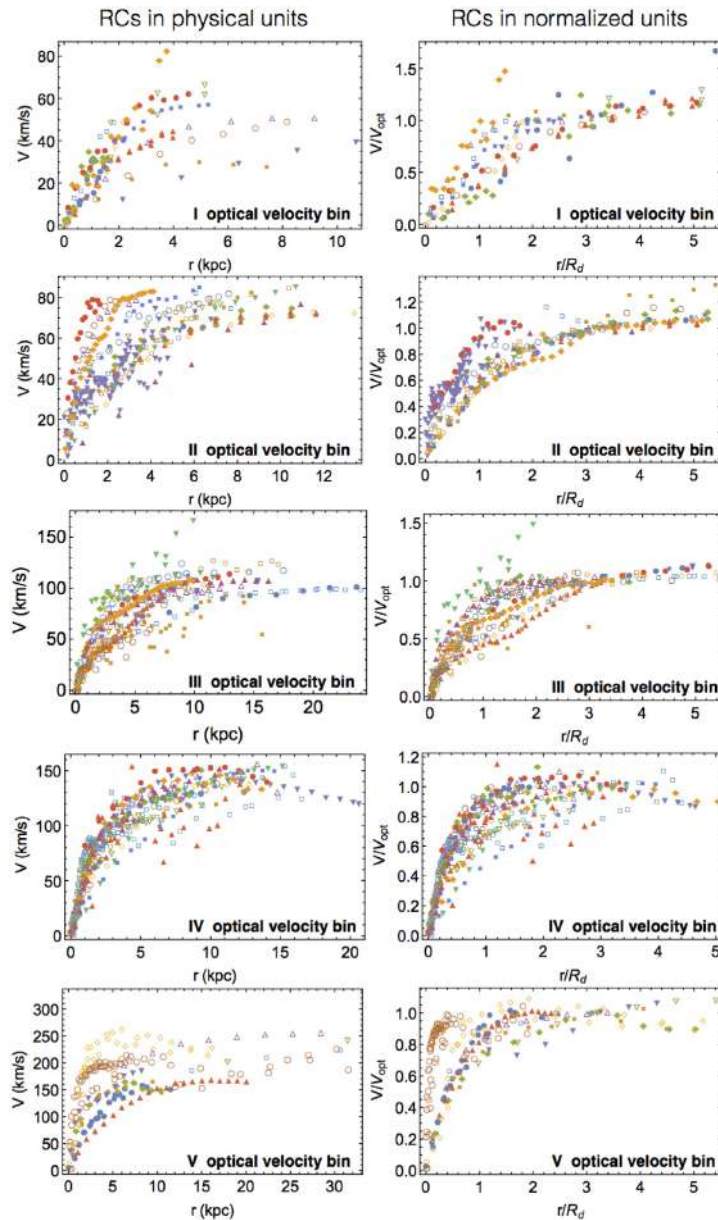


Figure D1. LSBs RCs belonging to each of the five optical velocity bins.

## APPENDIX E: CONSTRUCTION OF THE CO-ADDED ROTATION CURVES

In Tables E1–E2 we show the data related to the five co-added RCs obtained in Section 3. In detail, the first column describes the centre of the radial bins represented by the coloured points in Figs 5–7. The second column indicates the number of RCs data (grey points in Fig. 5) belonging to each radial bin. Finally, the third and the fourth columns show the velocity data and their error bars in physical units, related to the co-added RCs in the second panel of Fig. 6 and in Fig. 7.

**Table E1.** RCs for each optical velocity bin of LSB galaxies. Columns: (1) centre of the radial bin; (2) number of data in each bin; (3) co-added velocity for each bin; (4) velocity error. In order to express the radial coordinate in physical units, the data of the first column relative to each velocity bin must be multiplied by the respective average value of disc scale length  $\langle R_D \rangle$ , reported in Table 1.

$r/R_D$	N. data	$V$ $\text{km s}^{-1}$	Error bar $\text{km s}^{-1}$
(1)	(2)	(3)	(4)
I velocity bin			
0.2	15	7.3	1.2
0.6	19	16.7	1.7
1.0	18	25.6	2.4
1.4	19	34.2	3.1
1.8	13	37.1	1.6
2.25	13	42.4	1.4
2.75	10	41.9	2.1
3.25	13	45.5	0.9
3.75	5	48.4	0.7
4.25	5	51.1	1.4
4.75	5	49.9	1.1
5.25	5	56.4	4.2
II velocity bin			
0.2	62	25.0	1.5
0.6	70	40.0	1.3
1.0	39	52.0	1.9
1.4	26	56.5	1.9
1.8	26	62.3	1.2
2.25	23	64.8	1.3
2.75	23	70.7	0.8
3.25	16	74.3	0.5
3.75	15	76.3	1.2
4.25	12	78.6	1.4
4.75	12	81.0	1.6
5.25	9	81.7	2.1
III velocity bin			
0.2	86	25.3	1.8
0.6	56	53.7	1.9
1.0	46	71.8	2.7
1.4	45	81.1	2.8
1.8	35	89.9	3.2
2.25	39	93.6	1.3
2.75	29	97.2	1.7
3.25	20	101.3	0.5
3.75	10	104.0	0.8
4.25	8	106.9	1.0
4.75	10	107.8	1.4
5.25	6	107.9	2.0

**Table E2.** It continues from Table E1.

$r/R_D$	N. data	$V$ $\text{km s}^{-1}$	Error bar $\text{km s}^{-1}$
(1)	(2)	(3)	(4)
IV velocity bin			
0.2	141	47.9	2.2
0.6	81	90.4	2.0
1.0	54	112.2	2.6
1.5	58	121.8	2.2
2.1	41	128.6	3.1
2.7	28	133.7	2.9
3.3	17	136.0	2.5
3.9	9	138.9	3.0
4.7	8	129.5	2.8
V velocity bin			
0.2	71	127.1	7.2
0.6	32	148.7	6.1
1.	23	173.9	3.5
1.4	14	197.6	3.7
1.8	16	194.8	4.9
2.25	14	198.2	3.4
2.75	5	199.3	5.2
3.25	9	205.5	1.5
3.75	6	203.2	4.0
4.4	8	199.6	5.3
5.2	5	195.2	6.9

## APPENDIX F: THE GAS COMPONENT IN THE ROTATION CURVES

The gas disc component in galaxies is an additional component to the stellar disc and the DM halo giving a contribution to the circular velocities. At any rate, by performing a suitable test, it is possible to realize that the gas is (moderately) important only in the first optical velocity bin, where, in any case, in the inner regions the stellar component overcomes the gaseous one, while in the external region the DM component overcomes the gaseous one; thus, the gas component gives a modest contribution to the RC. In Fig. F1, for the first velocity bin co-added RC, we compare the mass–velocity model fit that includes the contribution from a H I disc with the velocity–mass model which does not. The estimated masses of the stellar disc and of the DM halo show, in the two cases, only a moderate change.

By modelling the co-added RC of the first  $V_{\text{opt}}$  bin by means of the stellar/H I disc + DM halo model we get:

$$M_d = 8.0 \times 10^8 M_\odot;$$

$$r_0 = 10.7 \text{ kpc};$$

$$\rho_0 = 3.2 \times 10^{-3} M_\odot \text{ pc}^{-3};$$

$$M_{\text{vir}} = 8.2 \times 10^{10} M_\odot;$$

$$M_{\text{HI}} = 1.0 \times 10^9 M_\odot.$$

By removing the gaseous disc, we get:

$$M_d = 8.8 \times 10^8 M_\odot;$$

$$r_0 = 10.7 \text{ kpc};$$

$$\rho_0 = 3.7 \times 10^{-3} M_\odot \text{ pc}^{-3};$$

$$M_{\text{vir}} = 1.0 \times 10^{11} M_\odot.$$

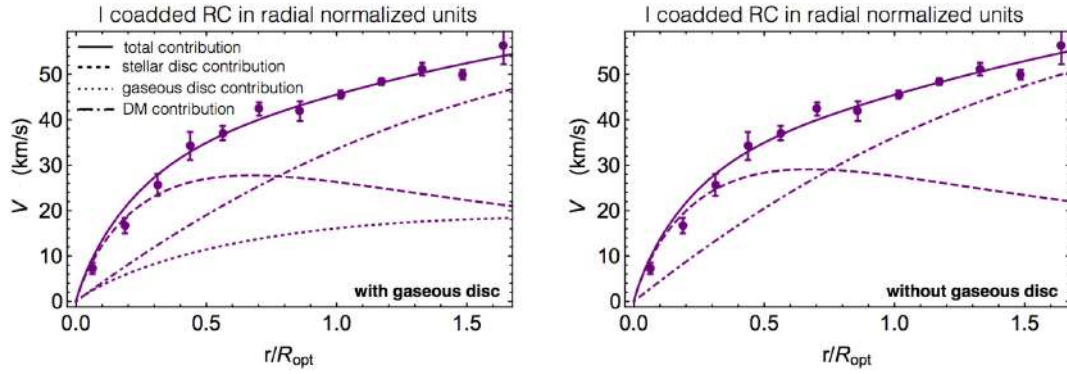


**Figure F1.** I velocity bin RC best fitted with gas (left-hand panel) and without gas (right-hand panel). The dashed, dot-dashed, dotted, and solid lines stand for the stellar disc, the DM halo, the gaseous disc, and the total contributions to the RC.

We remind that  $M_d$ ,  $r_0$ ,  $\rho_0$ ,  $M_{\text{HI}}$  (all quantities inferred by the fit) are the stellar disc mass, the DM halo core radius, the central core mass density, the HI gaseous disc mass (including the correction for the helium contribution), respectively.  $M_{\text{vir}}$  is the virial mass. The differences in the values of  $M_d$ ,  $r_0$ ,  $\rho_0$ ,  $M_{\text{vir}}$ , when we include gas or we exclude the gaseous component, are inside the error bars reported in Table 2 related to the fit without the HI disc.

## APPENDIX G: STRUCTURAL PROPERTIES OF LSB GALAXIES

In Tables G1–G2 we report: the names of the LSB galaxies in our sample alongside their distances  $D$ , the stellar disc scale lengths  $R_d$ , and the optical velocities  $V_{\text{opt}}$  (all taken from literature). Furthermore, the table shows the values of the stellar disc mass  $M_d$ , the DM core radius  $R_c$ , the central density of the DM halo  $\rho_0$ , the virial mass  $M_{\text{vir}}$ , the central surface density  $\Sigma_0 = \rho_0 R_c$ , the compactness of the stellar mass distribution  $C_*$ , and that of the DM mass distribution  $C_{\text{DM}}$ , all evaluated in this work.

**Table G1.** Individual properties of LSBs. Columns: (1) galaxy name; (2) distance; (3) disc scale length; (4) optical velocity; (5) disc mass; (6) core radius; (7) central DM density; (8) virial mass; (9) central surface density; (10) compactness of stellar mass distribution; (11) compactness of the DM mass distribution.

Name	$D$ Mpc	$R_d$ kpc	$V_{\text{opt}}$ $\text{km s}^{-1}$	$M_d$ $10^7 M_\odot$	$R_c$ kpc	$\text{Log } \rho_0$ $\text{g cm}^{-3}$	$M_{\text{vir}}$ $10^9 M_\odot$	$\text{Log } \Sigma_0$ $M_\odot \text{pc}^{-2}$	$\text{Log } C_*$	$\text{Log } C_{\text{DM}}$
(1)	(2)	(3)	(4)	(5)	(6)	(7)	(8)	(9)	(10)	(11)
UGC4115	7.8	0.4	24.2	6.3	1.1	-23.57	1.6	1.63	0.06	-0.15
F563V1	51.0	2.4	27.3	48	14	-25.30	27	1.01	-0.40	-0.57
UGC11583	5.9	0.3	27.9	6.5	0.7	-23.17	1.6	1.88	0.17	-0.00
UGC2684	8.2	0.8	36.7	29	2.9	-23.95	12	1.69	-0.00	-0.10
F574-2	66.0	4.5	40.0	192	33	-25.57	171	1.13	-0.45	-0.50
F565V2	36.0	2.0	45.2	110	11	-24.69	76	1.51	-0.19	-0.21
UGC5272	6.1	1.2	48.8	77	5.2	-24.11	42	1.77	-0.02	-0.04
UGC8837	5.1	1.2	49.6	79	5.2	-24.10	44	1.78	-0.02	-0.03
F561-1	63.0	3.6	50.8	250	25	-25.15	244	1.41	-0.31	-0.28
UGC3174	11.8	1.0	51.7	72	4.0	-23.88	36	1.89	0.04	0.04
NGC 4455	6.8	0.9	53.0	68	3.4	-23.75	33	1.96	0.08	0.08
UGC1281	5.5	1.7	55.0	138	8.5	-24.36	96	1.74	-0.08	-0.05
UGC1551	20.2	2.5	55.8	211	15	-24.73	182	1.61	-0.18	-0.14
UGC9211	12.6	1.3	61.9	165	5.9	-24.10	66	1.84	0.06	0.01
F583-1	1.6	1.6	62.0	201	7.8	-24.29	90	1.77	0.00	-0.03
UGC5716	24.1	2.0	66.4	288	11	-24.45	150	1.75	-0.03	-0.04
UGC7178	24.0	2.3	69.9	367	13	-24.54	210	1.74	-0.06	-0.04
ESO400-G037	37.5	4.1	69.9	651	29	-25.09	502	1.55	-0.21	-0.18
NGC 3274	0.47	0.5	68.0	75	1.5	-23.01	18	2.33	0.35	0.30
F583-4	49.0	2.7	70.5	438	16	-24.69	275	1.69	-0.10	-0.08
F571V1	79.0	3.2	72.4	549	21	-24.83	382	1.66	-0.14	-0.10
NGC 5204	4.9	0.7	73.1	115	2.2	-23.24	33	2.27	0.30	0.27
UGC731	8.0	1.7	73.3	298	8.5	-24.20	147	1.90	0.04	0.05
NGC 959	7.8	0.9	75.3	172	3.6	-23.57	60	2.15	0.21	0.21
NGC 100	11.2	1.2	77.2	233	5.2	-23.81	96	2.07	0.15	0.16
NGC 5023	4.8	0.8	78.4	160	2.9	-23.38	52	2.25	0.27	0.27
UGC5750	56.0	5.6	80.0	1171	46	-25.27	1125	1.56	-0.26	-0.18
UGC3371	12.8	3.1	82.0	681	20	-24.69	494	1.78	-0.09	-0.02

**Table G1** – *continued*

Name	$D$ Mpc	$R_d$ kpc	$V_{\text{opt}}$ km s <sup>-1</sup>	$M_d$ 10 <sup>7</sup> M <sub>⊙</sub>	$R_c$ kpc	Log $\rho_0$ g cm <sup>-3</sup>	$M_{\text{vir}}$ 10 <sup>9</sup> M <sub>⊙</sub>	Log $\Sigma_0$ M <sub>⊙</sub> pc <sup>-2</sup>	Log $C_*$	Log $C_{\text{DM}}$
(1)	(2)	(3)	(4)	(5)	(6)	(7)	(8)	(9)	(10)	(11)
NGC 4395	3.5	2.3	82.3	509	13	-24.40	312	1.89	-0.00	0.05
UGC11557	23.8	3.1	83.7	710	20	-24.67	520	1.80	-0.08	-0.01
UGC1230	51.0	4.5	90.0	1278	34	-24.99	1027	1.71	-0.15	-0.07
ESO206-G014	60.3	5.2	91.3	1531	42	-25.12	1338	1.67	-0.19	-0.10
NGC 2552	10.1	1.6	92.0	475	7.8	-23.97	213	2.09	0.14	0.18
UGC4278	10.5	2.3	92.6	691	13	-24.32	386	1.96	0.04	0.10
UGC634	35.0	3.1	95.1	984	20	-24.59	662	1.88	-0.03	0.05
ESO488-G049	23.0	4.4	95.3	1410	33	-24.92	1159	1.76	-0.13	-0.03
UGC5005	52.0	4.4	95.5	1406	33	-24.92	1153	1.77	-0.13	-0.03
UGC3137	18.4	2.0	97.7	669	11	-24.14	350	2.06	0.10	0.17
F574-1	96.0	4.5	99.0	1546	34	-24.91	1306	1.79	-0.12	-0.01
F568-3	77.0	4.0	100.5	1416	29	-24.78	1130	1.84	-0.08	0.02
ESO322-G019	45.2	2.5	100.7	878	14	-24.32	528	2.01	0.05	0.14
F563V2	61.0	2.1	101.3	755	11	-24.15	412	2.07	0.10	0.18
NGC 247	2.5	2.9	106.6	1156	18	-24.42	784	2.00	0.02	0.13
ESO444-G021	60.7	6.4	107.4	2603	56	-25.17	2760	1.75	-0.19	-0.05
F579V1	85.0	5.1	111.5	2223	40	-24.92	2134	1.85	-0.12	0.03
F568V1	80.0	3.2	115.8	1505	21	-24.44	1119	2.04	0.02	0.16
ESO374-G003	43.2	4.2	118.3	2084	31	-24.70	1856	1.97	-0.05	0.11
F568-1	85.0	5.3	130.0	4218	43	-25.13	1354	1.67	-0.03	-0.10
UGC628	65.0	4.7	130.0	3740	36	-25.02	1132	1.71	0.00	-0.07
UGC11616	72.8	4.9	133.2	4094	38	-25.04	1282	1.71	-0.00	-0.07
ESO186-G055	60.1	3.6	133.2	3041	25	-24.76	813	1.81	0.08	0.00
ESO323-G042	59.7	4.4	138.7	4020	33	-24.91	1221	1.78	0.04	-0.02
PGC37759	193.2	6.8	139.4	6195	60	-25.30	2318	1.65	-0.08	-0.12
ESO234-G013	60.9	3.7	139.4	3425	26	-24.74	949	1.84	0.08	0.02
F571-8	48.0	5.2	139.5	4765	42	-25.05	1577	1.73	-0.00	-0.05
F730V1	144.0	5.8	141.6	5523	49	-25.15	1953	1.71	-0.03	-0.07
UGC11648	46.7	3.8	142.2	3620	27	-24.74	1022	1.85	0.09	0.03
ESO215-G039	61.3	4.2	142.9	4037	31	-24.83	1208	1.82	0.06	0.01
ESO509-G091	72.8	3.7	146.8	3735	25	-24.68	1050	1.89	0.11	0.06

**Table G2.** It continues from Table G1.

Name	$D$ Mpc	$R_d$ kpc	$V_{\text{opt}}$ km s <sup>-1</sup>	$M_d$ 10 <sup>7</sup> M <sub>⊙</sub>	$R_c$ kpc	Log $\rho_0$ g cm <sup>-3</sup>	$M_{\text{vir}}$ 10 <sup>9</sup> M <sub>⊙</sub>	Log $\Sigma_0$ M <sub>⊙</sub> /pc <sup>2</sup>	Log $C_*$	Log $C_{\text{DM}}$
(1)	(2)	(3)	(4)	(5)	(6)	(7)	(8)	(9)	(10)	(11)
ESO444-G047	62.4	2.7	148.4	2809	16	-24.38	662	2.01	0.19	0.13
UGC11454	92.1	4.5	150.3	4787	34	-24.85	1525	1.85	0.06	0.03
UGC5999	45.0	4.4	153.0	4851	33	-24.82	1540	1.87	0.07	0.04
UGC11819	59.2	5.3	154.6	6578	43	-25.10	1490	1.70	0.04	-0.08
ESO382-G006	65.4	2.3	160.0	3097	13	-24.29	449	2.01	0.27	0.13
ESO323-G073	69.6	2.1	165.3	2923	11	-24.14	398	2.08	0.32	0.18
NGC 3347B	46.2	8.1	167.0	11760	78	-25.43	3369	1.63	-0.05	-0.14
ESO268-G044	49.9	1.9	175.6	3057	10	-24.01	406	2.16	0.36	0.23
ESO534-G020	226.7	16.7	216.6	40638	218	-25.86	17351	1.64	-0.17	-0.18
NGC 7589	115.0	12.6	224.0	32831	146	-25.58	13657	1.75	-0.08	-0.07
UGC11748	73.1	3.1	240.7	9418	20	-24.22	1911	2.26	0.32	0.31
UGC2936	43.6	8.4	255.0	28363	82	-25.09	10784	1.99	0.07	0.12
F568-6	201.0	18.3	297.0	83839	249	-25.67	49173	1.89	-0.10	0.01

**APPENDIX H: ERRORS AND SCATTER IN THE SCALING RELATIONS**

In Table H1, the errors on the best-fitting parameters of the scaling relations evaluated in this work are shown. The standard scatter  $\sigma$  of individual galaxies data of the various scaling relations is also reported. In the 2D scaling relations, it is evaluated according to:

$\sigma = \sqrt{\sum_{i=1}^N (y_i - f(x_i))^2 / N}$ , where  $N = 72$ ,  $y_i$  and  $x_i$  are the logarithmic data in the  $y$  and  $x$  axes, respectively, and  $f$  is the considered scaling function (a line). In the 3D scaling relations, the standard

scatter is evaluated according to:  $\sigma = \sqrt{\sum_{i=1}^N (z_i - \tilde{f}(x_i, y_i))^2 / N}$ , where  $z_i$ ,  $y_i$ ,  $x_i$  are the logarithmic data in the  $z$ ,  $y$ , and  $x$  axes, respectively, and  $\tilde{f}$  is the considered scaling function (a plane).

**APPENDIX I: LSB ROTATION CURVES WITH THEIR URC**

We show in Figs II–I5 the LSBs RCs data together with their URC, taking into account equations (21) and (22) and the values of  $R_{\text{opt}} \equiv 3.2 R_d$ ,  $V_{\text{opt}}$ , and  $C_*$  reported in Tables G1–G2 in Appendix G. We also show the URC for the case  $\text{Log } C_* = 0$  in Figs II–I5. In comparing the URC model with the 72 individual RCs, in 21 of them we have assumed a random systematic error running from  $\simeq 3$  per cent to  $\simeq 16$  per cent in their amplitudes (velocity measurements). In Table II, the changes applied are specified. Removing such systematics improves fits which were already successful. Let us stress that the URC can help determining how well an individual RC correctly reflects the mass distribution of the galaxy.

**Table H1.** Errors and scatters on the various scaling relations. Columns: (1) relation; (2)–(4) error bars on the *first*, *second*, and *third* (when present) fitting parameters; (5) standard scatter of the 72 individual galaxies data from the scaling relations.

Fitted relation (1)	$\Delta a$ (2)	$\Delta b$ (3)	$\Delta c$ (4)	$\sigma$ (5)
Equation (9): $\text{Log } R_c(\text{Log } R_d)$	0.15	0.26	–	–
Equation (14): $\text{Log } M_d(\text{Log } V_{\text{opt}})$	0.25	0.12	–	0.24
Equation (15): $\text{Log } \rho_0(\text{Log } R_c)$	0.07	0.05	–	0.21
Equation (17): $\text{Log } R_d(\text{Log } V_{\text{opt}})$	0.25	0.13	–	0.24
Equation (17): $\text{Log } R_c(\text{Log } V_{\text{opt}})$	0.36	0.18	–	0.34
Equation (17): $\text{Log } \rho_0(\text{Log } V_{\text{opt}})$	0.56	0.28	–	0.54
Equation (18): $\text{Log } R_d(\text{Log } M_d)$	0.23	0.02	–	0.16
Equation (20): $\text{Log } M_d(\text{Log } V_{\text{opt}}, \text{Log } C_*)$	0.06	0.03	0.04	0.06
Equation (20): $\text{Log } R_d(\text{Log } V_{\text{opt}}, \text{Log } C_*)$	0.02	0.01	0.02	0.02
Equation (20): $\text{Log } R_c(\text{Log } V_{\text{opt}}, \text{Log } C_*)$	0.03	0.02	0.02	0.03
Equation (20): $\text{Log } \rho_0(\text{Log } V_{\text{opt}}, \text{Log } C_*)$	0.15	0.07	0.10	0.13
Equation (23): $\text{Log } R_c(\text{Log } M_{\text{vir}})$	0.26	0.02	–	0.15
Equation (24): $\text{Log } C_*(\text{Log } C_{\text{DM}})$	0.01	0.06	–	0.15

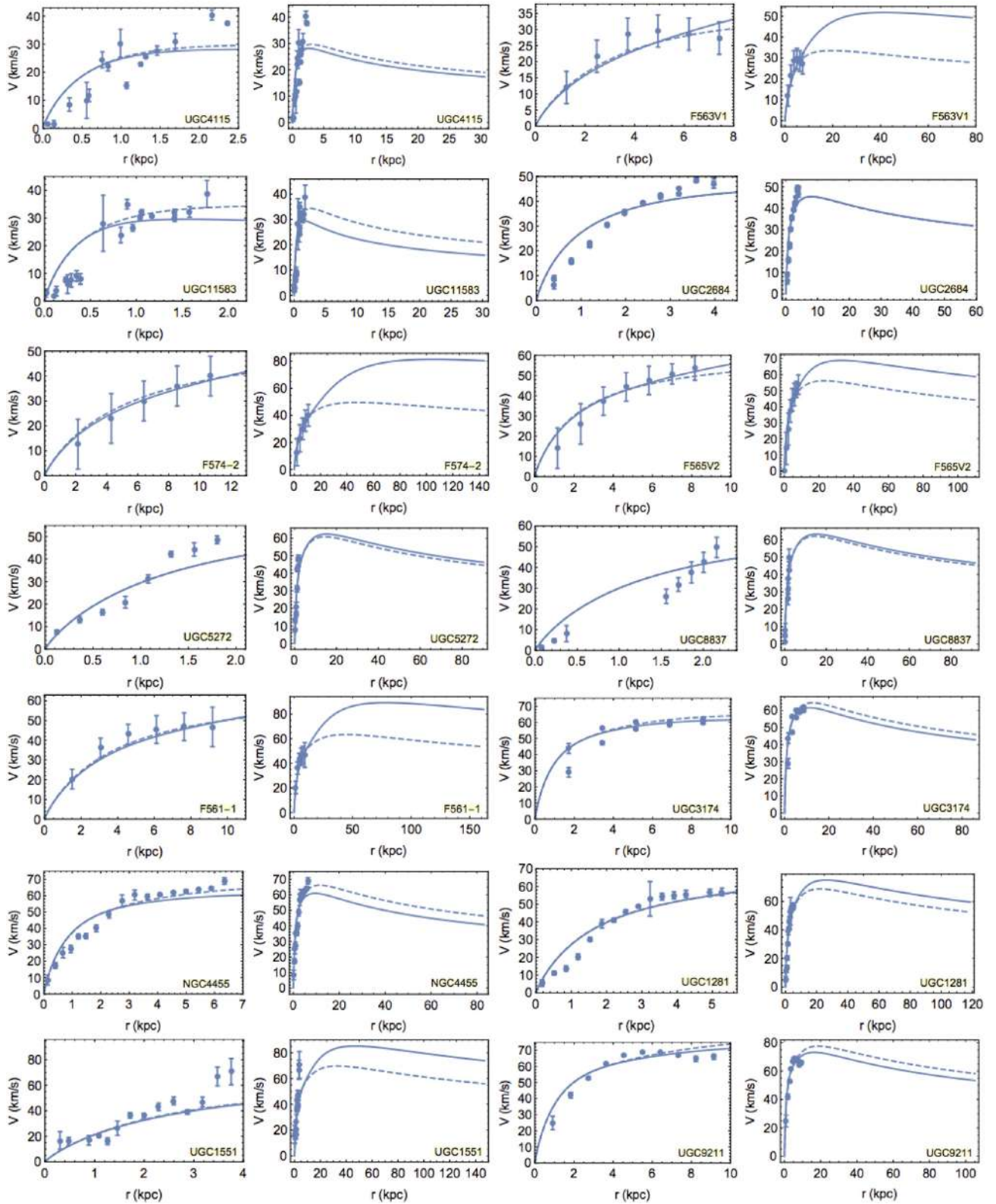


**Figure 11.** LSBs RCs data with their URC given by equations (21)–(22). The *solid* line is obtained for the  $\text{Log } C_*$  values reported in Tables G1–G2 in Appendix G and is compared with the *dashed* line obtained for  $\text{Log } C_* = 0$ . For each galaxy, we show the URC fit up to the farthest measurements (*left*) and up to the virial radius (*right*).

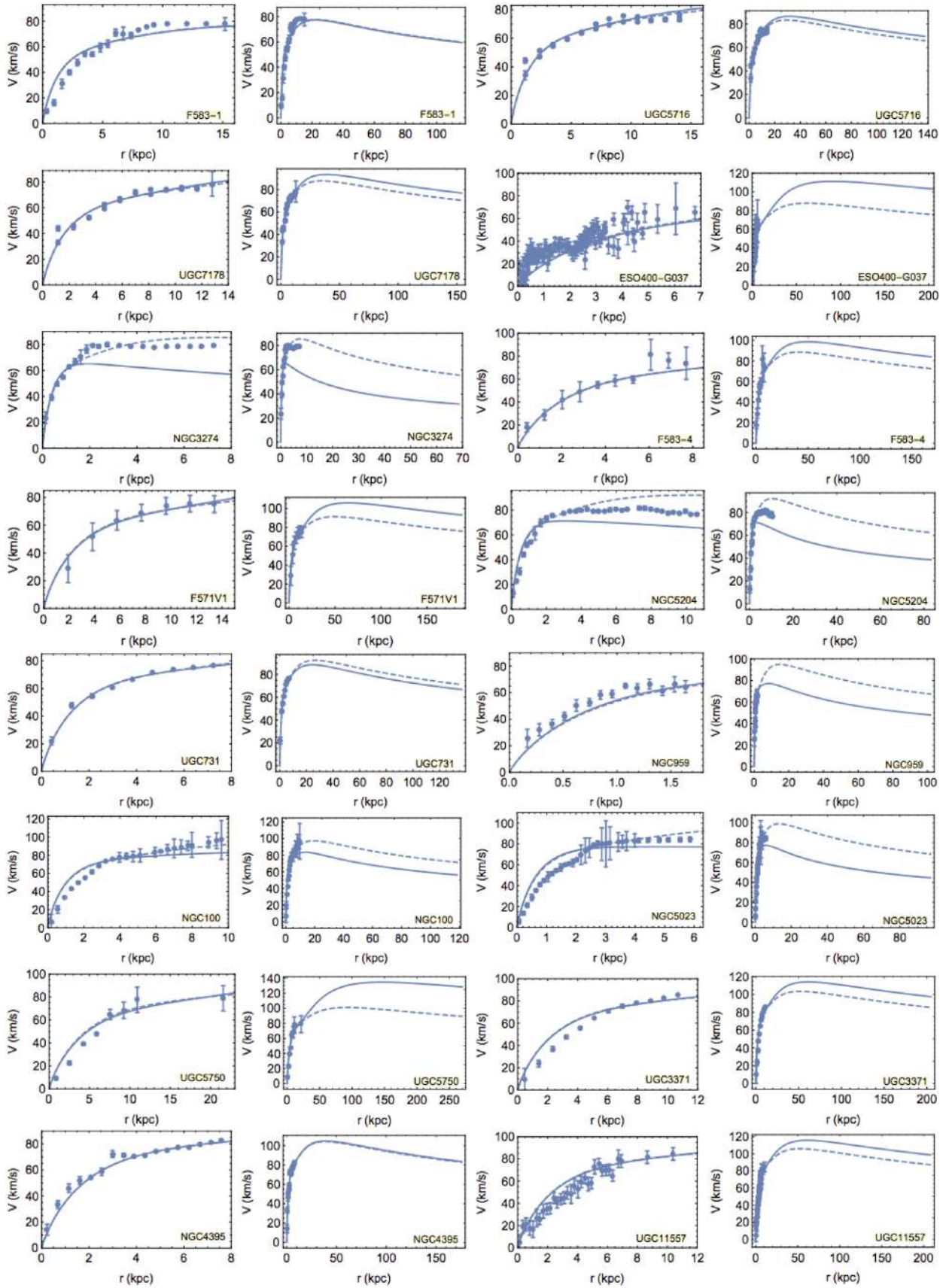


Figure 12. It continues from Table 11.

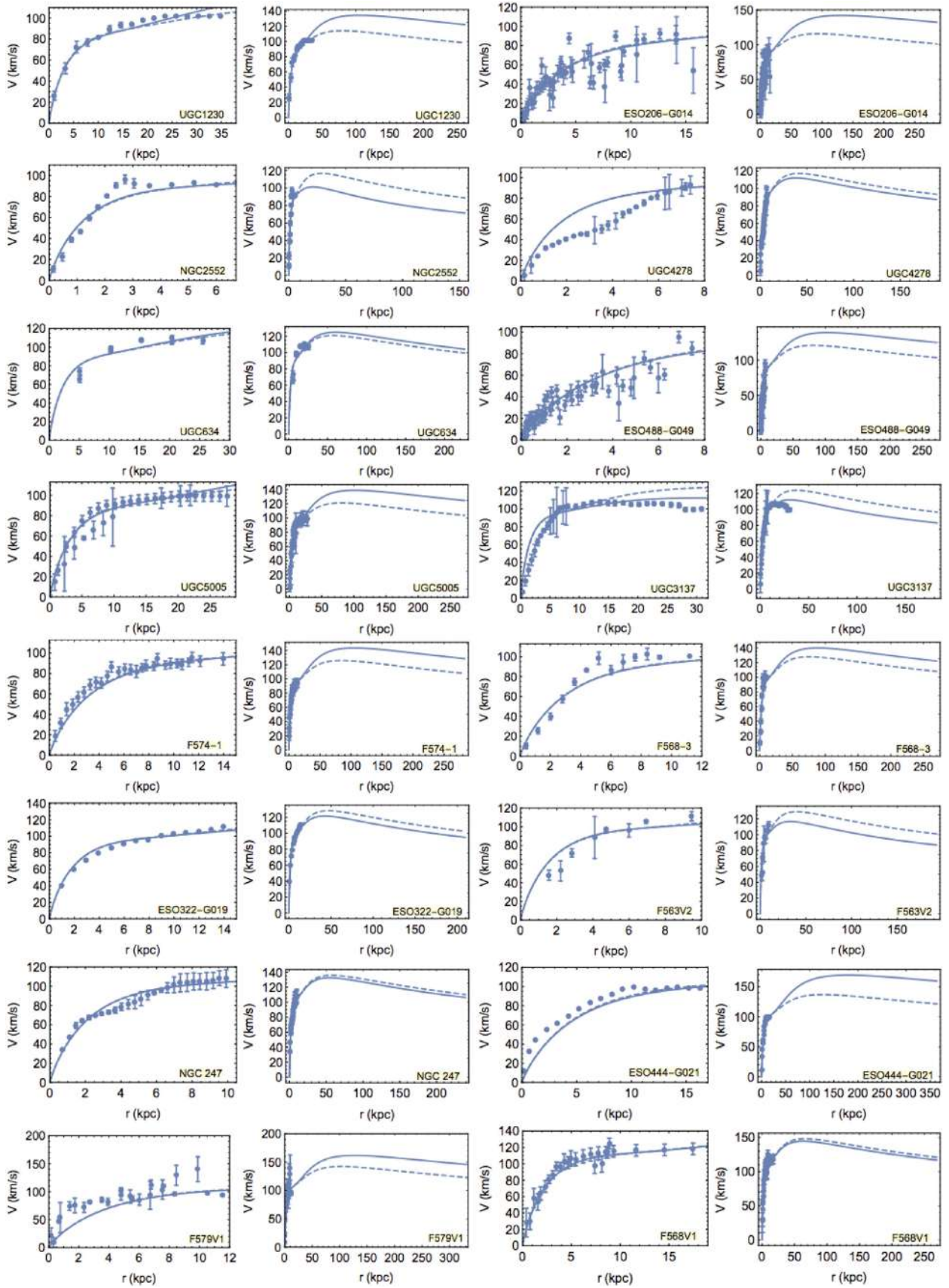


Figure I3. It continues from Table I2.

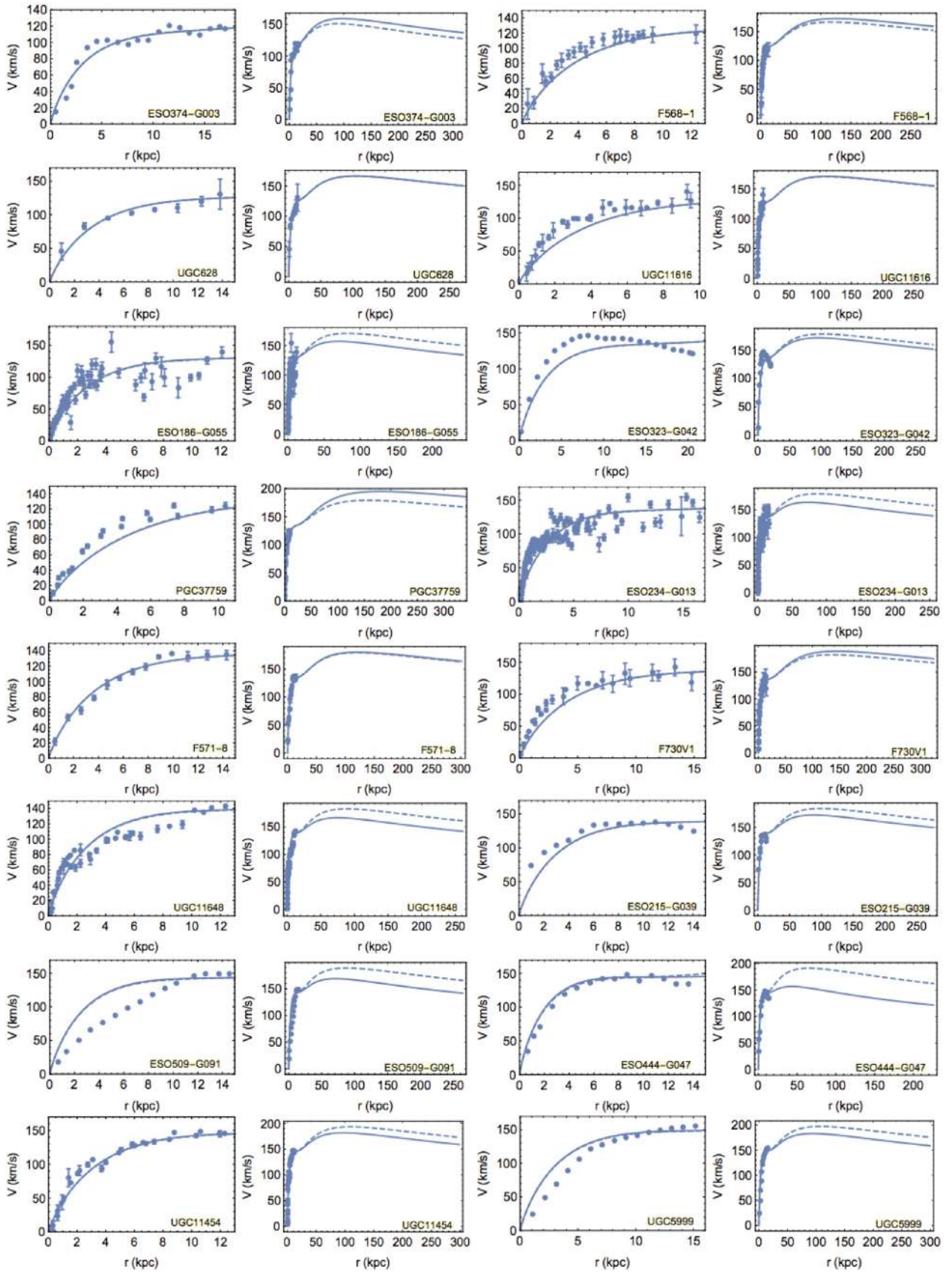


Figure 14. It continues from Table I3.

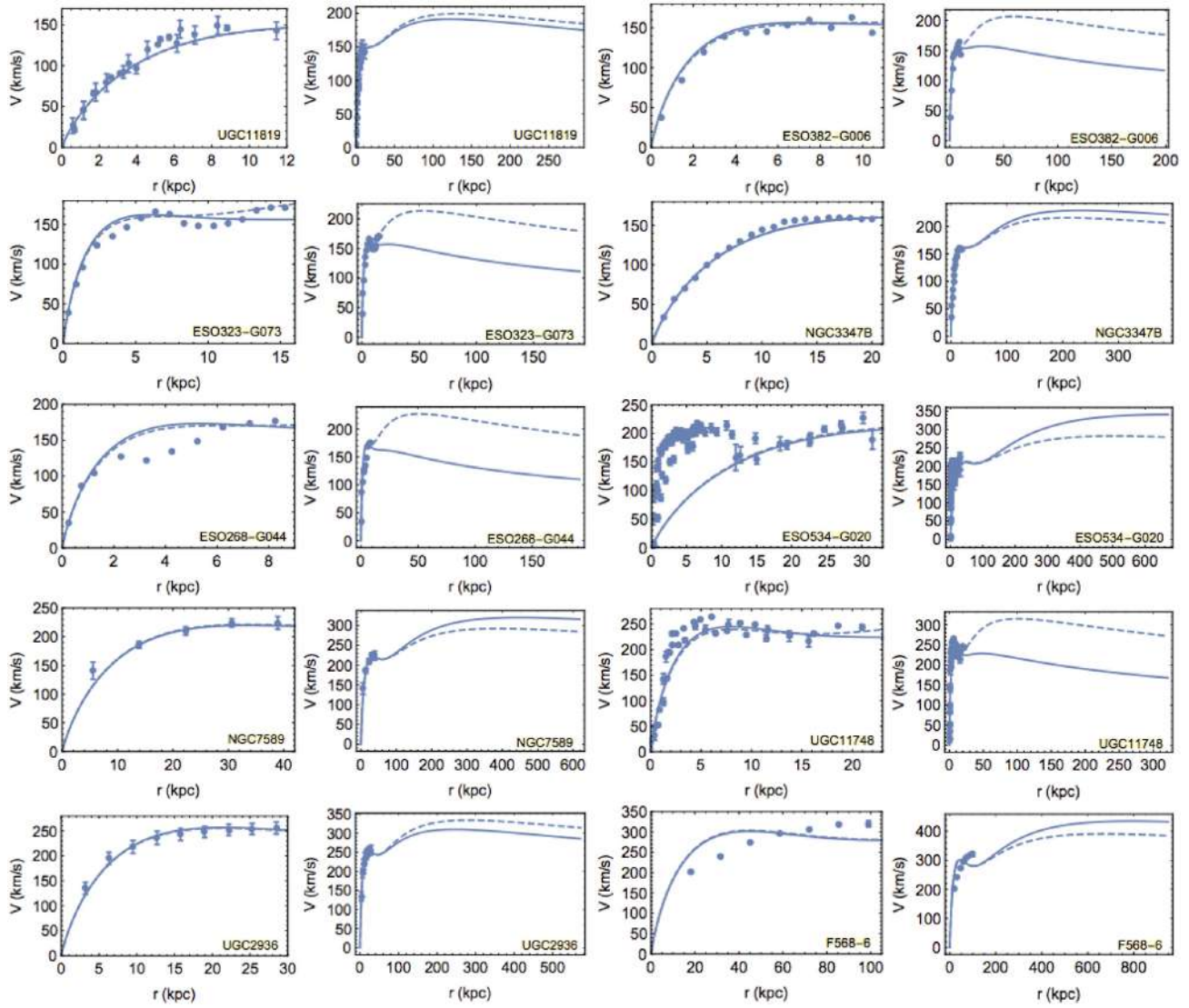


Figure 15. It continues from Table 14.

**Table 11.** List of galaxies in which we have left the amplitude of the RC to freely vary by  $f$  per cent. Columns: (1) galaxy name; (2) correction to the velocity values of the RCs data, expressed in  $f$  per cent.

Name (1)	$f$ per cent (2)
UGC2684	+ 10.9
F565V2	+ 8.8
F561-1	- 7.9
UGC3174	- 9.7
UGC1551	- 14.3
UGC9211	+ 4.8
F583-1	- 8.1
ESO400-G037	- 7.1
NGC 959	- 15.9
F574-1	- 8.1
ESO444-G021	- 9.3
F579V1	- 16.1
ESO374-G003	- 5.9
F568-1	- 9.2
UGC11616	- 7.5
PGC37759	- 10.8
F730V1	- 9.2
ESO215-G039	- 10.5
UGC11454	- 3.3
NGC 3347B	- 6.0
ESO268-G044	- 5.7

This paper has been typeset from a  $\text{\TeX}/\text{\LaTeX}$  file prepared by the author.